Neuron

Article

Interaction of an α-synuclein epitope with HLA-DRB1*15:01 triggers enteric features in mice reminiscent of prodromal Parkinson's disease

Graphical abstract

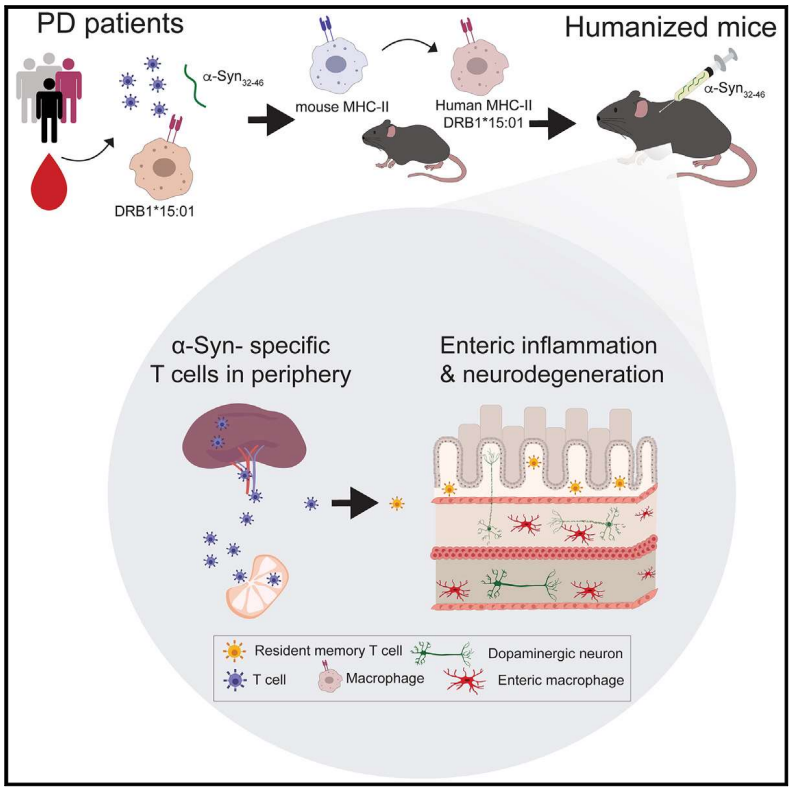

Highlights

- α-syn$_{32-46}$ immunization of HLA-DRB1*15:01 mice triggers weight loss and constipation
- α-syn$_{32-46}$ immunizations induce inflammation and neuron loss in the gut
- Depletion of CD4$^+$, but not CD8$^+$, T cells partially rescues enteric neural loss
- Both α-syn$_{32-46}$ and HLA-DRB1*15:01 are critical for this model of prodromal PD

Authors

Francesca Garretti, Connor Monahan, Nicholas Sloan, ..., Ellen Kanter, Dritan Agalliu, David Sulzer

Correspondence

da191@cumc.columbia.edu (D.A.), ds43@cumc.columbia.edu (D.S.)

In brief

Parkinson's disease (PD) patients exhibit elevated numbers of T cells that recognize α-synuclein (α-syn) epitopes, particularly in early disease. One epitope, α-syn$_{32-46}$, interacts with the HLA-DRB1*15:01; however, its role in PD pathogenesis remains unknown. Garretti et al. show that α-syn$_{32-46}$ immunization of a mouse expressing HLA-DRB1*15:01 triggers intestinal inflammation, enteric neurodegeneration, constipation, and weight loss, suggesting a critical role for α-syn autoimmunity in HLA-DRB1*15:01 carriers in prodromal PD.

Garretti et al., 2023, Neuron *111*, 3397–3413
November 1, 2023
https://doi.org/10.1016/j.neuron.2023.07.015

CellPress

Neuron

CellPress
OPEN ACCESS

Article

Interaction of an α-synuclein epitope with HLA-DRB1*15:01 triggers enteric features in mice reminiscent of prodromal Parkinson's disease

Francesca Garretti,[1,2,10,11,12] Connor Monahan,[2,10,11] Nicholas Sloan,[3] Jamie Bergen,[3,4] Sanjid Shahriar,[1] Seon Woo Kim,[5] Alessandro Sette,[6,7,10] Tyler Cutforth,[8,10] Ellen Kanter,[2,9] Dritan Agalliu,[1,8,10,*] and David Sulzer[2,8,9,10,13,*]

[1]Department of Pathology and Cell Biology, Columbia University Irving Medical Center, New York, NY, USA
[2]Departments of Psychiatry and Pharmacology, Columbia University Irving Medical Center, New York, NY, USA
[3]Department of Neuroscience, Columbia University, New York, NY, USA
[4]Department of Computer Science, Columbia University, New York, NY, USA
[5]Weill Cornell Medicine - Qatar, Education City, Doha, Qatar
[6]Division of Vaccine Discovery, La Jolla Institute for Immunology, La Jolla, CA, USA
[7]Department of Medicine, University of California in San Diego, San Diego, CA, USA
[8]Department of Neurology, Columbia University Irving Medical Center, New York, NY, USA
[9]Division of Molecular Therapeutics, New York State Psychiatric Institute, New York, NY, USA
[10]Aligning Science Across Parkinson's (ASAP) Collaborative Research Network, Chevy Chase, MD, USA
[11]These authors contributed equally
[12]Present address: Department of Genetics and Genomics, Icahn School of Medicine at Mount Sinai, New York, NY, USA
[13]Lead contact
*Correspondence: da191@cumc.columbia.edu (D.A.), ds43@cumc.columbia.edu (D.S.)
https://doi.org/10.1016/j.neuron.2023.07.015

SUMMARY

Enteric symptoms are hallmarks of prodromal Parkinson's disease (PD) that appear decades before the onset of motor symptoms and diagnosis. PD patients possess circulating T cells that recognize specific α-synuclein (α-syn)-derived epitopes. One epitope, α-syn$_{32-46}$, binds with strong affinity to the HLA-DRB1*15:01 allele implicated in autoimmune diseases. We report that α-syn$_{32-46}$ immunization in a mouse expressing human HLA-DRB1*15:01 triggers intestinal inflammation, leading to loss of enteric neurons, damaged enteric dopaminergic neurons, constipation, and weight loss. α-Syn$_{32-46}$ immunization activates innate and adaptive immune gene signatures in the gut and induces changes in the CD4$^+$ T$_H$1/T$_H$17 transcriptome that resemble tissue-resident memory (T$_{RM}$) cells found in mucosal barriers during inflammation. Depletion of CD4$^+$, but not CD8$^+$, T cells partially rescues enteric neurodegeneration. Therefore, interaction of α-syn$_{32-46}$ and HLA-DRB1*15:0 is critical for gut inflammation and CD4$^+$ T cell-mediated loss of enteric neurons in humanized mice, suggesting mechanisms that may underlie prodromal enteric PD.

INTRODUCTION

Parkinson's disease (PD) is a neurodegenerative disorder characterized by prominent motor symptoms resulting from the loss of central nervous system (CNS) dopaminergic neurons in the substantia nigra (SN).[1] However, its pathogenesis begins long before diagnosis, and CNS neuronal death is suspected to occur at relatively late stages of disease. In contrast, enteric nervous system (ENS) symptoms are common during an earlier stage of the disease.[2] Constipation presents in approximately 70% of PD patients,[3] is 3-fold more prevalent in PD patients than healthy controls,[4] and occurs as early as 20 years prior to the onset of motor symptoms.[5] Although epidemiological studies demonstrate a high prevalence of constipation in PD patients (reviewed in Fasano et al.[3]), and postmortem studies indicate that gut pathology is present before the onset of motor symptoms,[6,7] the mechanisms underlying the enteric pathophysiology remain unclear.

Braak and colleagues have hypothesized that α-synuclein (α-syn)-mediated pathology begins in the ENS and ascends rostrally into the brain via the vagus nerve.[6] This conjecture is consistent with reports that truncal vagotomies decrease the risk for PD.[8–10] Epidemiological studies support a role for gut inflammation in early stages of PD. The incidence of PD among patients with inflammatory bowel disease (IBD) is 28% higher than controls. Furthermore, IBD patients who receive anti-tumor necrosis factor alpha (TNF-α) therapy exhibit a 78%–100% reduction in PD incidence compared with those who do not receive such therapy.[11,12] Multiple observations in animal models indicate that gut inflammation may be involved in the early stages of PD (reviewed in Metzger et al.[13]).

Peripheral inflammation is likely implicated in PD pathogenesis because high levels of pro-inflammatory cytokines (e.g., TNF-α, interleukin [IL]-1β, IL-6, and interferon [IFN]γ) are found in PD patients and correlate negatively with disease duration.[14–17] PD patients also possess circulating T cells, mostly $CD4^+$ subtypes, which recognize specific α-syn-derived neo-epitopes.[18] These cells are abundant in the first decade after diagnosis and likely during the prodromal phase.[19] Thus, α-syn neo-antigen reactivity is relevant to the prodromal and early stages of PD (reviewed in Garretti et al.[20]). However, the role of α-syn neo-antigen reactivity in disease etiology remains unknown.

Previously, we reported that most α-syn-responsive $CD4^+$ T cells isolated from PD patients respond to epitopes derived from two regions of the protein.[18] One region requires the presence of phosphorylated serine 129,[18] a post-translational modification present at high levels in Lewy bodies.[21] However, these C-terminal epitopes bind weakly to several human leukocyte antigen (HLA, reviewed in Dendrou et al.[22]) alleles, although they still may be immunogenic. The other major α-syn epitope identified in PD patients is an $\alpha\text{-syn}_{32\text{-}46}$ peptide, which lies in proximity to several rare α-syn mutations that cause familial PD.[23–31] In contrast to C-terminal epitopes, the $\alpha\text{-syn}_{32\text{-}46}$ epitope is highly restricted to DRB5*01 and DRB1*15:01 HLA alleles, a type II histocompatibility complex, and binds them with a strong binding affinity (K_D = 2.8 nM) *in vitro*.[18] Genome-wide association studies (GWASs) have also confirmed these HLA alleles in a haplotype associated with PD.[32–34]

It is unknown how the interaction between this α-syn epitope ($\alpha\text{-syn}_{32\text{-}46}$) and HLA allele (DRB1*15:01) may trigger early features of PD. Here, we report that $\alpha\text{-syn}_{32\text{-}46}$ immunizations of a mouse strain lacking major histocompatibility complex class II (MHCII) and expressing the human HLA-DRB1*15:01 allele trigger intestinal inflammation and loss of enteric neurons in the submucosal plexus (SP) of the small intestine, leading to transient constipation and weight loss, with no detectable effects in the CNS. Bulk RNA sequencing (RNA-seq) of the gut reveals that $\alpha\text{-syn}_{32\text{-}46}$ immunizations induce innate and adaptive immune responses and IFN signaling. Single-cell RNA-seq (scRNA-seq) of immune cells showed altered gene signatures in $CD4^+$ T_H1 and T_H17 lamina propria lymphocytes from complete Freund's adjuvant (CFA)/$\alpha\text{-syn}_{32\text{-}46}$-immunized mice, characteristic of antigen-experienced tissue-resident memory (T_{RM}) cells found in mucosal barriers during infection and chronic inflammation. Depletion of $CD4^+$, but not $CD8^+$, T cells partially rescued enteric neurodegeneration. Thus, interactions of $\alpha\text{-syn}_{32\text{-}46}$ with the HLA-DRB1*15:01 allele are critical for the induction of enteric features resembling those seen in prodromal PD, suggesting that additional hits (e.g., blockade of intracellular protein turnover and/or α-syn aggregation) may be required for the development of CNS symptoms.

RESULTS

$\alpha\text{-Syn}_{32\text{-}46}$ immunizations cause illness marked by severe weight loss and constipation in HLA-DRB1*15:01, but not WT, mice

Previously, we have shown that $CD4^+$ T cells isolated from PD patients carrying the HLA-DRB1*15:01 allele confer a strong immune response to the $\alpha\text{-syn}_{32\text{-}46}$ region of the protein.[18] To test whether these anti-$\alpha\text{-syn}_{32\text{-}46}$ immune responses can produce features of PD pathology in mice, we performed active immunizations by adapting a protocol similar to the myelin oligodendrocyte glycoprotein ($MOG_{35–55}$) experimental autoimmune encephalomyelitis (EAE) mouse model for human multiple sclerosis (MS).[35,36] Mice were immunized with either PBS with CFA or $\alpha\text{-syn}_{32\text{-}46}$ with CFA (referred to as CFA and CFA/$\alpha\text{-syn}_{32\text{-}46}$ immunization, respectively). As in EAE, *Bordetella pertussis* toxin (PTx) was administered intravenously 14 and 16 days post-initial immunization (DPI) with the boost to transiently open the blood-brain barrier in order to permit immune cell infiltration into the CNS (Figure 1A). In addition, mice were injected with PBS alone to control for the effects of CFA administration (referred to herein as PBS). These immunizations were performed either in C57BL/6J (referred to as wild type [WT]) mice, or a humanized mouse strain lacking mouse MHCII alleles and expressing the human HLA-DRB1*15:01 allele (referred to as the HLA mice[37,38]) (Figure 1A). We confirmed that splenocytes from HLA-DRB1*15:01 mice expressed HLA-DR protein and that its expression was increased after lipopolysaccharide (LPS) exposure (Figures S1A–S1G). HLA-DR protein was not detected in WT splenocytes, as expected (Figures S1H and S1I). In addition, we confirmed that HLA mice expressed proportions of $CD4^+$ and $CD8^+$ T cells similar to WT mice (Figures S1J–S1L).

Mice were monitored daily for overt signs of malaise or weight changes (Figures 1B–1E). Mice were categorized as "sick" if they lost more than 12% of the initial body weight and exhibited hunched posture with ungroomed and "ruffled" fur (Figure 1B). Following immunizations, very few WT mice became sick, regardless of the immunization antigen (0% of CFA, 4% CFA/$\alpha\text{-syn}_{32\text{-}46}$; Figures 1B and 1C). In contrast, while CFA alone produced no illness in HLA mice, 25% of HLA mice immunized with CFA/$\alpha\text{-syn}_{32\text{-}46}$ became ill or died (Figures 1B and 1D). The "sick" CFA/$\alpha\text{-syn}_{32\text{-}46}$-immunized HLA mice exhibited severe weight loss, which started at 16 DPI and peaked at 22–24 DPI, with a mean weight change of −15.68% at 22 DPI ($p = 0.0272$; Figure 1E). The weight effects following CFA/$\alpha\text{-syn}_{32\text{-}46}$ immunization were specific to HLA mice and absent in WT mice (Figure 1C). This phenotype was transient: sick immunized HLA mice restored their initial weight between 24 and 29 DPI, with no further weight gain (Figure 1E).

Because constipation is often an early symptom associated with PD that occurs as early as 20 years prior to the onset of motor symptoms,[5] we assessed total gastrointestinal (GI) transit time in either PBS-, CFA-, or CFA/$\alpha\text{-syn}_{32\text{-}46}$-immunized mice by measuring the time required for a non-absorbable red dye to be excreted with feces after oral administration (Figures 2A and 2B). We selected three time points after immunization (21, 25, and 35 DPI) to correlate this phenotype with the weight loss (Figure 1E). Immunizations with CFA had a significant effect on total GI transit time (PBS vs. CFA, $p = 0.0029$; PBS vs. CFA/$\alpha\text{-syn}_{32\text{-}46}$, $p < 0.0001$; Figures 2C and 2D). Although the GI transit time between all CFA/$\alpha\text{-syn}_{32\text{-}46}$- and CFA-immunized HLA mice at 21 DPI was not significantly different ($p = 0.1473$; Figure 2C), the sick CFA/$\alpha\text{-syn}_{32\text{-}46}$-immunized HLA mice displayed significantly longer GI transit time compared with both PBS- and CFA-immunized mice ($p < 0.0001$; Figure 2D). The

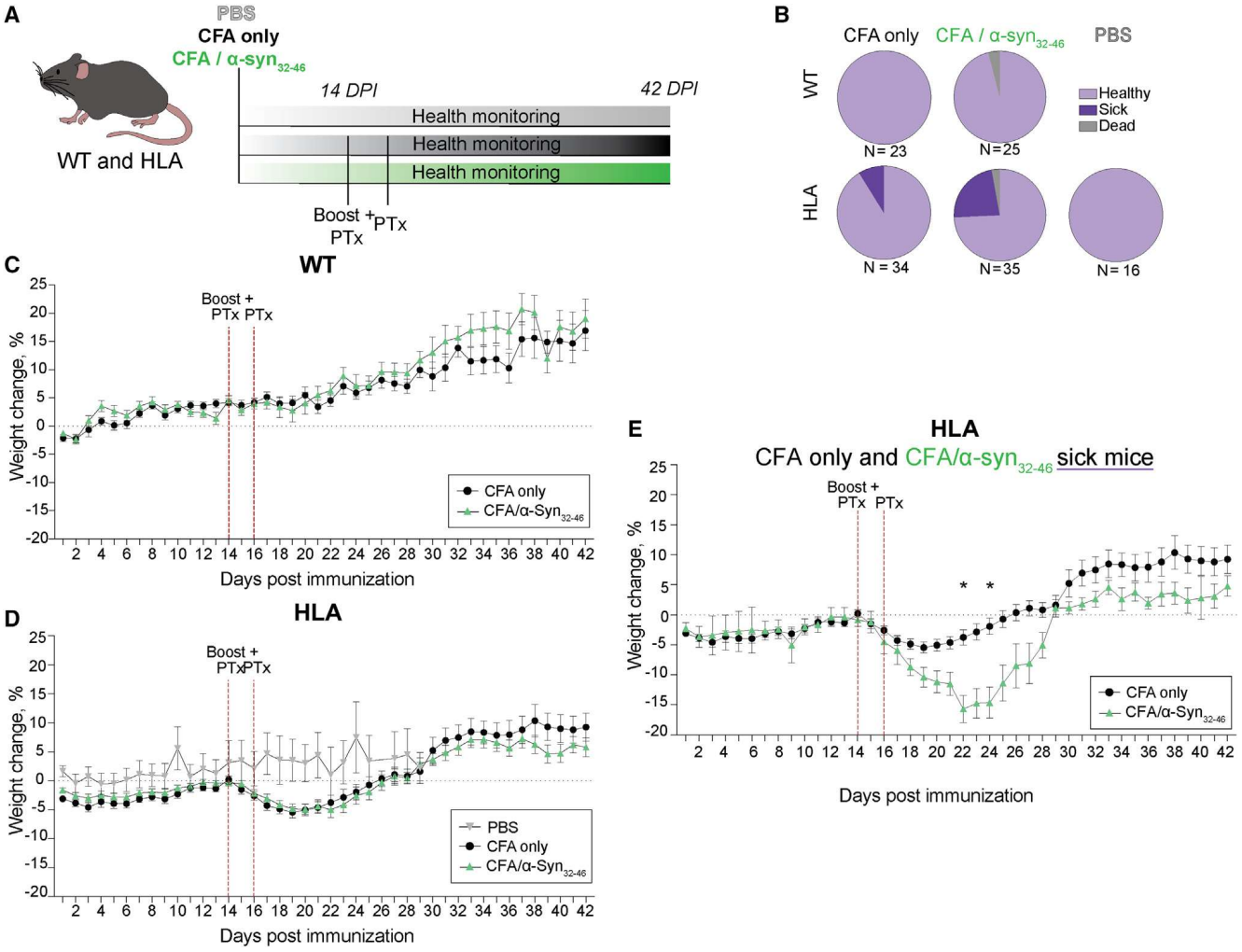

Figure 1. α-syn$_{32-46}$ immunizations induce weight loss in HLA-DRB1*15:01, but not wild-type, mice

(A) A schematic diagram of the experimental design.

(B) Pie charts show the fraction of immunized WT (top) and HLA (bottom) mice that were healthy (light purple), became ill (dark purple), or died (gray).

(C and D) Graphs of percentage weight change from the initial weight (0 DPI) for WT (C) and HLA (D) mice immunized with either PBS (gray triangles), CFA only (black circles), or CFA/α-syn$_{32-46}$ (green triangles). The red dashed lines indicate the time when mice received an immunization boost and PTx injections at 14 and 16 DPI, respectively.

(E) Graph depicting the percentage of weight loss for CFA-only- and sick CFA/α-syn$_{32-46}$-immunized HLA mice. The data in (E) were analyzed using a mixed-effect ANOVA for repeated measurements followed by Bonferroni post hoc correction; *p < 0.05. WT: CFA only (n = 23 mice), CFA/α-syn$_{32-46}$ (n = 25 mice). HLA: PBS (n = 16 mice), CFA only (n = 34 mice), CFA/α-syn$_{32-46}$ (n = 35 mice). See also Figure S1.

increase in GI transit time, however, normalized by 25 and 35 DPI (Figures 2E and 2F), mirroring the recovery from weight loss (Figure 1E). Interestingly, all CFA/α-syn$_{32-46}$ HLA mice showed a significant negative correlation between the peak weight loss and GI transit time ($r = -0.5643$, $p = 0.0077$; Figure 2H), whereas this was not seen with CFA-immunized HLA mice (peak weight loss and GI transit time; $r = 0.3188$, $p = 0.1707$; Figure 2G). In contrast, all immunized WT mice exhibited unaltered total GI transit times, regardless of the immunization antigen, indicating a specificity of the immune response (Figure 2I). Thus, the combination of α-syn$_{32-46}$ and HLA-DRB1*15:01 allele expression induces acute GI illness (weight loss and constipation) between 22 and 24 DPI.

α-Syn$_{32-46}$-immunized HLA mice exhibit loss of enteric, but not CNS, neurons

The weight loss associated with constipation observed in CFA/α-syn$_{32-46}$-immunized HLA mice suggests a pathological response targeting the gut. To examine the gut histopathology underlying these phenotypes, we prepared flat mounts of both the submucosal (SPs) and myenteric (MPs) plexuses of the ileum (small intestine) from immunized HLA mice at 28 DPI (Figures 3A and 3B), as this preparation provides an in-depth analysis of the ENS. We focused in particular on the SP because it is directly exposed to circulating immune cells and has the highest concentration of dopaminergic neurons.[39] To investigate whether the increase in total GI transit time was associated with neuronal loss,

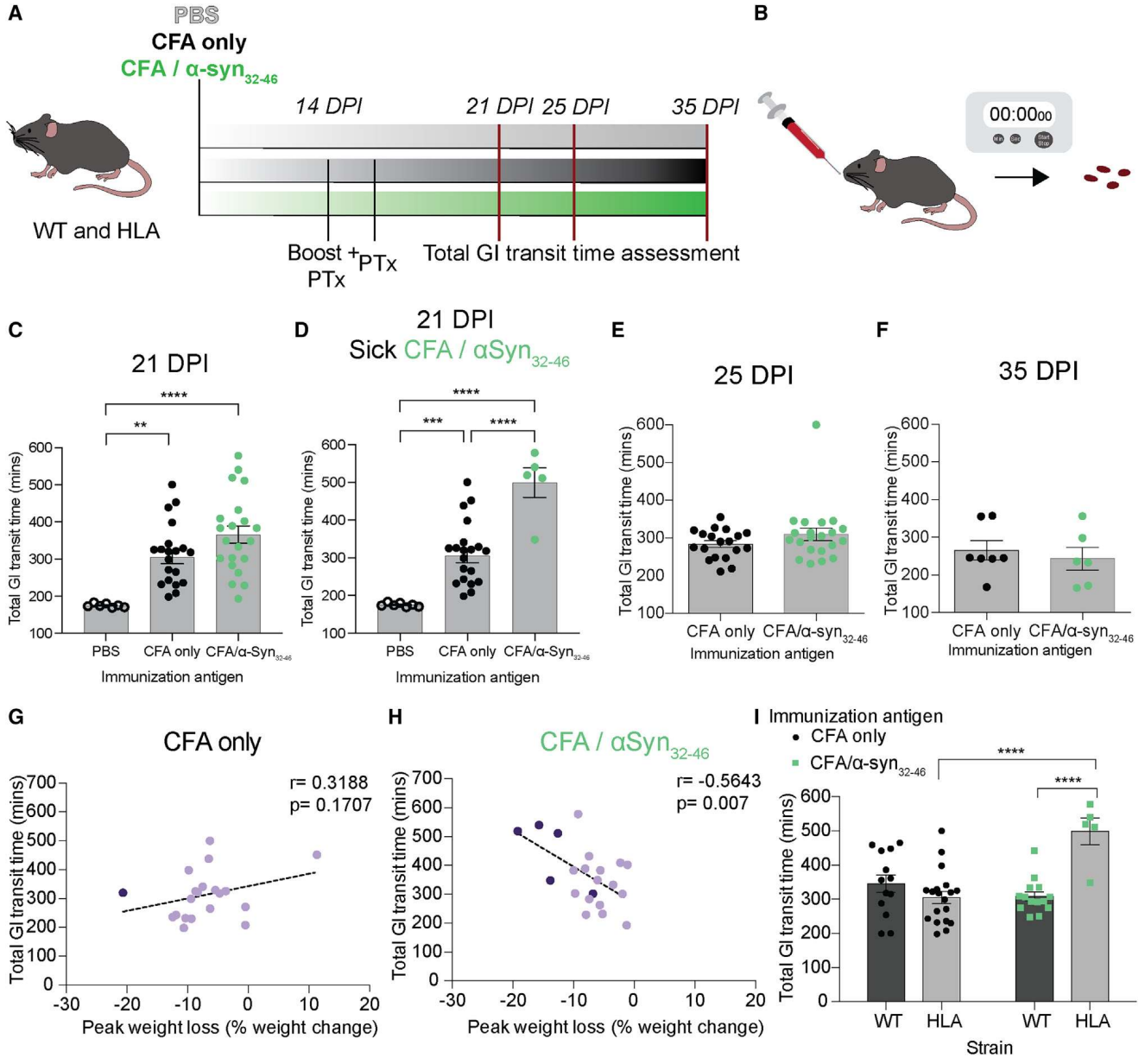

Figure 2. Total GI transit time is delayed in CFA/α-syn$_{32-46}$-immunized HLA mice

(A and B) Diagrams of the experimental design for immunization and GI transit time.

(C and D) Dotted bar graphs of total GI transit time at 21 DPI for all (C) and sick (D) HLA mice immunized with PBS (empty circles), CFA only (black), and CFA/α-syn$_{32-46}$ (green).

(E and F) Dotted bar graphs of total GI transit time of CFA-only- (black) and CFA/α-syn$_{32-46}$-immunized (green) HLA mice at 25 (E) and 35 (F) DPI.

(G and H) Correlation graphs between peak weight loss and total GI transit time of CFA-only- (G) and CFA/α-syn$_{32-46}$-immunized (H) HLA mice. Dark purple circles represent sick and light purple circles represent healthy mice.

(I) Bar graphs of the total GI transit time of WT (dark bars) and HLA (light bars) immunized with CFA only (black) or CFA/α-syn$_{32-46}$ (green). Only sick CFA/α-syn$_{32-46}$-immunized HLA mice are shown. Data were analyzed by Mann-Whitney test (C and D), Pearson correlation (G and H), and two-way ANOVA (I); $^{**}p < 0.01$, $^{***}p < 0.001$, $^{****}p < 0.0001$. Dotted bar graphs represent the mean and SEM. Each symbol represents data from one animal. WT: CFA only, n = 13 mice; CFA/α-syn$_{32-46}$, n = 14 mice. HLA: PBS, n = 7 mice; CFA only, n = 20 mice; CFA/α-syn$_{32-46}$, n = 21 mice. WT: 2 independent experiments; HLA: 5 independent experiments. See also Figure S2.

we analyzed the expression of ANNA1 as a marker for enteric neuronal nuclei and tyrosine hydroxylase (TH) as a marker for catecholaminergic neurons, which in the ileum are mostly dopaminergic.[39]

In the MP, there was a similar density of ANNA1$^+$ neurons among PBS-, CFA-, and CFA/α-syn$_{32-46}$-immunized HLA mice (Figures 3C–3E and 3I). CFA immunization reduced the overall TH$^+$ neuron density in the MP (PBS vs. CFA, p = 0.005; PBS

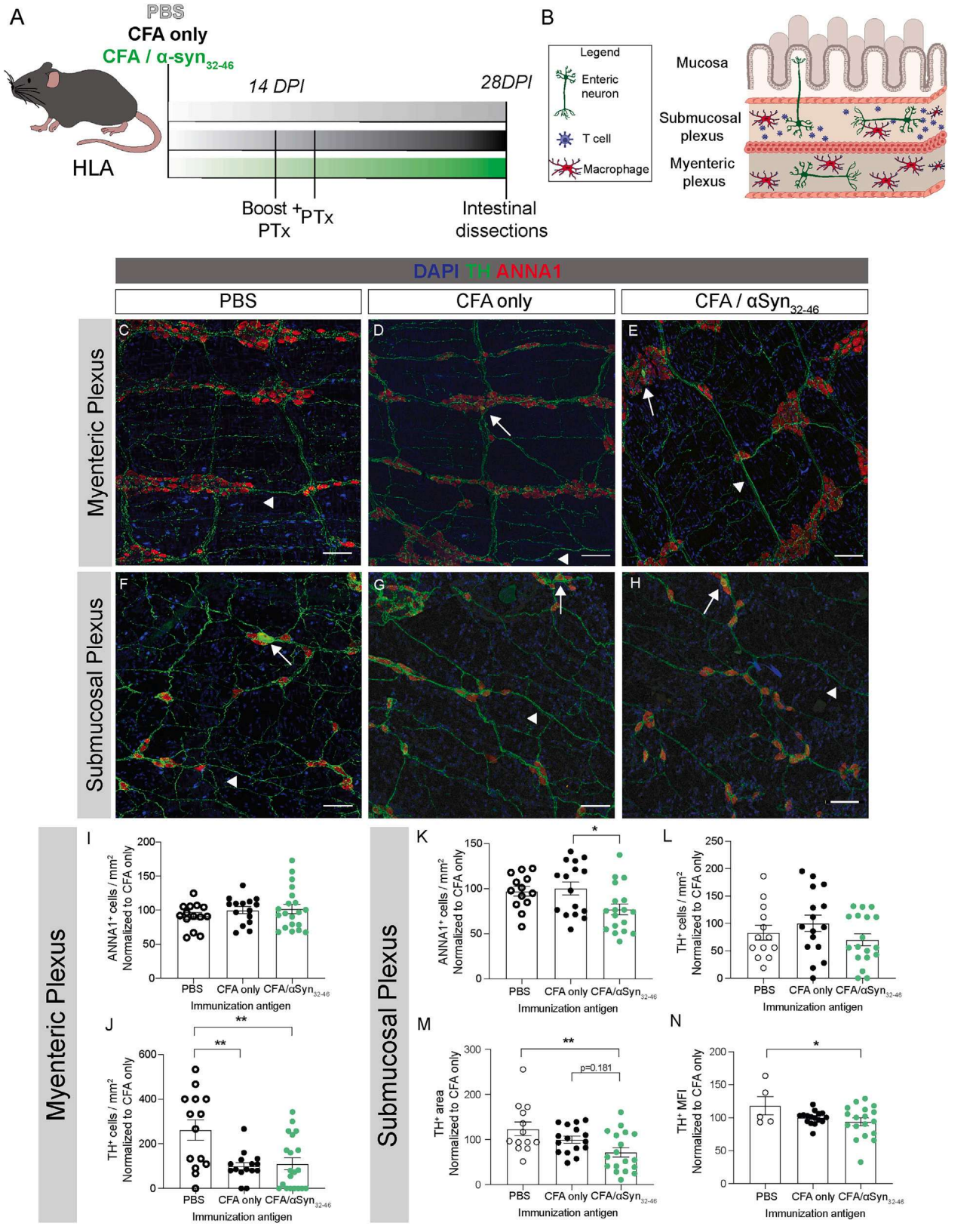

(legend on next page)

vs. CFA/α-syn$_{32-46}$, p = 0.006; Figure 3J), consistent with adjuvant effects on total GI transit time (Figures 2C and 2D). In contrast, CFA/α-syn$_{32-46}$-immunized HLA mice exhibited a significantly reduced ANNA1$^+$ neuronal density in the SP compared with CFA-immunized HLA mice (p = 0.04, Figures 3F–3H and 3K), with no significant difference between PBS- and CFA-immunized mice (Figure 3K). There was no significant difference in the number of TH$^+$ neurons within the SP in any group (Figure 3L, p = 0.260), which may be due to the variable density of TH$^+$ neurons within the ENS. Importantly, the area of TH$^+$ processes was significantly lower in CFA/α-syn$_{32-46}$-immunized compared with PBS-injected HLA mice (Figure 3M, p = 0.008), with no significant difference between CFA- and CFA/α-syn$_{32-46}$-immunized HLA mice (Figure 3M; p = 0.181). Similarly, the mean fluorescent intensity (MFI) of TH label within neuronal cell bodies and processes 28 DPI was significantly lower in CFA/α-syn$_{32-46}$-immunized than PBS HLA mice (Figure 3N, p = 0.017), without a significant difference between CFA- and CFA/α-syn$_{32-46}$-immunized HLA mice (Figure 3N; p = 0.171). The effects of CFA/α-syn$_{32-46}$ immunizations on enteric neuronal loss were specific to HLA mice and not seen in WT mice (Figure S2). Thus, α-syn$_{32-46}$ immunizations induced loss of enteric neurons in the ileum only in the HLA-DRB1*15:01 strain.

The SP is exposed to circulating immune cells (Figure 3B).[40] To determine whether the enteric neuron loss observed in CFA/α-syn$_{32-46}$-immunized HLA mice correlates with immune cell infiltration, we immunolabeled and quantified Iba1$^+$/CD68$^+$ macrophages in both layers (Figure S3). We found no significant difference in CD68$^+$ macrophage density in either the MPs (Figures S3A–S3C and S3G) or the SPs (Figures S3D–S3F and S3H) of the HLA mice, regardless of the immunizing condition. Thus, the loss of enteric neurons does not correlate with the macrophage number in CFA/α-syn$_{32-46}$-immunized HLA mice.

Next, we examined whether CFA/α-syn$_{32-46}$-immunized HLA mice exhibiting weight loss and constipation had CNS pathology. α-Syn$_{32-46}$ immunizations did not induce CD3$^+$ T cell infiltration, microglia activation, macrophage infiltration, or loss of SN dopaminergic neurons in the brains of either WT or HLA mice, up to 2 months after immunization (70 DPI; Figures S4A–S4O). Consistently, neither WT nor HLA mice displayed motor behavior or learning deficits after α-syn$_{32-46}$ immunizations (Figures S4P–S4Y). The lack of CNS lymphocyte infiltration, neuroinflammation, and neurodegeneration coupled with no changes in either motor skills or learning behaviors indicate that the severe weight loss and constipation in α-syn$_{32-46}$-immunized HLA mice are likely not related to changes in basal ganglia circuits. Therefore, the responses to α-syn$_{32-46}$ immunizations were restricted to the ENS in HLA mice.

Dopaminergic neuron damage in the gut persists after weight loss in α-syn$_{32-46}$-immunized HLA mice

To uncover the chronology between weight loss, gut inflammation and ENS neuronal death in CFA/α-syn$_{32-46}$-immunized HLA mice, we analyzed the number of ANNA1$^+$ and TH$^+$ neurons in the MPs and SPs 18 and 42 DPI (Figures 4A and 4B), prior to and after the weight loss (Figure 1E). At 18 DPI, there was no difference in the number of ANNA1$^+$ neurons, dopaminergic neurons, or TH$^+$ fluorescence signals in the SP between CFA- and CFA/α-syn$_{32-46}$-immunized HLA mice (Figures 4E, 4F, and 4I–4L). At 42 DPI, the area and MFI of the TH$^+$ signal were both significantly decreased in the SP of CFA/α-syn$_{32-46}$- compared with CFA-immunized HLA mice (p = 0.0135 and p = 0.0066, respectively; Figures 4O, 4P, 4U, and 4V), with no significant difference in ANNA1$^+$ or dopaminergic TH$^+$ neurons (p = 0.226; Figures 4O, 4P, 4S, and 4T). There were no changes in either of the neuronal parameters in the MP (Figures 4C, 4D, 4G, 4H, 4M, 4N, 4Q, and 4R), or the number of macrophages in both plexuses at 18 and 42 DPI between groups (Figures S3I–S3T), suggesting no relationship between macrophage number and ENS neuron loss. Thus, the damage of TH$^+$ dopamine neurons in the SP of CFA/α-syn$_{32-46}$-immunized HLA mice began prior to 28 DPI and persisted by day 42 DPI, after the mice had recovered from the weight loss, independent of macrophage infiltration in the gut.

α-Syn$_{32-46}$ immunization activates innate and adaptive immune gene signatures in the gut

To investigate the mechanisms underlying gut inflammation in CFA/α-syn$_{32-46}$-immunized HLA mice, we performed bulk RNA-seq of the ileum from CFA/α-syn$_{32-46}$- and CFA-immunized HLA mice at 21 DPI, when mice showed the largest weight loss (Figure 5A; Table S1). Differential gene expression analysis identified 143 upregulated and 54 downregulated genes in CFA/α-syn$_{32-46}$-immunized HLA mice (Figure 5B; $p_{adj} < 0.05$ and $|\log_2$ fold change [FC]$| > 0.5$; Tables S1B–S1D). Gene ontology (GO) enrichment analysis using the Database for Annotation, Visualization and Integrated Discovery (DAVID) revealed significant GO terms for genes with similar functional characteristics upregulated in CFA/α-syn$_{32-46}$-immunized HLA mice, such as: (1) the innate immune response (e.g., GO: 0045087, FDR = 2.34×10^{-25}); (2) the response to IFNβ (GO: 0035456, FDR = 3.64×10^{-15}), including IFN-stimulated genes (*Stat1/2*, *Oas2*, *Irf7*, and *Isg15*) that play multiple roles in defense against pathogens; and (3) the response to cytokines (GO: 0034097, FDR = 3.54×10^{-16}), including several chemokines (e.g., *Cxcl10* and *Cxcl13*) and *Vcam1*, a molecule involved in immune cell adhesion to blood vessels (Figure 5C; Table S1E). Genes involved in lymphocyte-mediated immunity (GO: 0002449,

Figure 3. α-Syn$_{32-46}$ immunizations induce enteric neuron loss in HLA-DRB1*15:01 mice

(A and B) Diagrams of the experimental design and the myenteric plexus (MP) and submucosal plexus (SP) of the ileum used for flat mount analysis.

(C–H) Representative images of the MP (C–E) and SP (F–H) stained for 4′,6-diamidino-2-phenylindole (DAPI,blue), TH (green), and ANNA1 (red). Thin white arrows indicate cell bodies of dopaminergic neurons; white arrowheads indicate dopaminergic neuronal processes. Scale bars, 75 μm.

(I–N) Dotted bar graphs of ANNA1$^+$ (I) and TH$^+$ (J) neurons per mm^2 in the MP; ANNA1$^+$ (K), TH$^+$ (L) neurons per mm^2, and area covered (M) and MFI (N) of the TH signal in the SP of PBS- (clear), CFA-only- (black), and CFA/α-syn$_{32-46}$-immunized (green) HLA mice. Dotted bar graphs show the mean and error bars the SEM. Data were analyzed by one-way ANOVA test. *p < 0.05, **p < 0.01. HLA mice: PBS, n = 14; CFA only, n = 15 mice; CFA/α-syn$_{32-46}$, n = 20 (myenteric) and 18 (submucosal); data collected from 6 independent experiments. See also Figure S3.

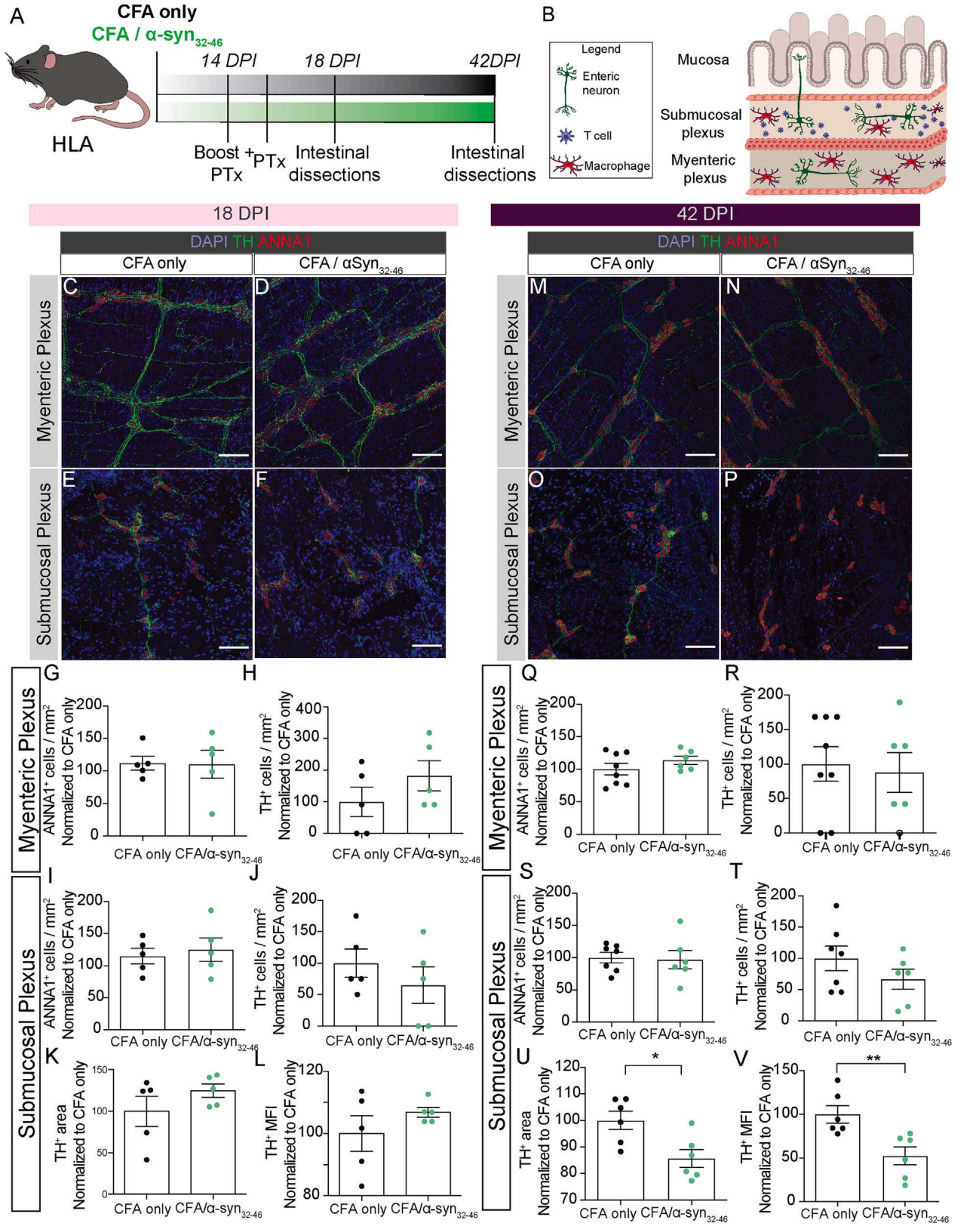

(legend on next page)

FDR = 0.00593) were also significantly enriched, including antigen processing and presentation via MHCI (*Tap1*, *H2.T24*, *H2.Q6*, *H2.T22*, *H2.T23*) (Figure 5C; Table S1E). Finally, humoral immune response was a significant GO term (GO: 0002455, FDR = 0.0495), with upregulation of genes encoding for the immunoglobulin heavy chain and complement cascade (Figure 5C; Table S1E). Thus, CFA/α-syn$_{32-46}$ immunizations upregulated innate and adaptive immune gene signatures in the ileum of HLA mice at peak weight loss and constipation.

α-Syn$_{32-46}$-specific T cells are present in the lymphatic organs of WT mice, but not HLA-DRB1*15:01 mice, after immunization

Because CFA/α-syn$_{32-46}$ immunizations upregulate innate and adaptive immune gene signatures in the ileum of HLA mice, we examined the antigen-specific adaptive immune response. We isolated primary cells from either the spleen or cervical and axillary lymph nodes of WT and HLA mice 28 DPI after immunizations with either CFA or CFA/α-syn$_{32-46}$ (Figure S5A). Cells were stimulated *in vitro* for 48 h with either α-syn$_{32-46}$, PBS or concanavalin A (ConA), as respective negative and positive controls. We then measured IFNγ and IL-17A levels, secreted by T_H1 and T_H17 lymphocytes, which are also elevated in the blood of PD patients.[41,42] α-Syn$_{32-46}$ and ConA induced IFNγ and IL-17A secretion from WT splenocytes and lymph cells, but had no effect on cells from CFA- and CFA/α-syn$_{32-46}$-immunized HLA mice ($p = 0.0691$; Figures S5B, S5C, S5G, and S5H; data not shown). The low levels of IFNγ in CFA/α-syn$_{32-46}$-immunized HLA mice were released primarily by $CD4^-$ $CD8^-$ cells ($p < 0.0001$), in contrast to the response of WT splenocytes after *in vitro* re-stimulation with α-syn$_{32-46}$, which was largely driven by $CD4^+$ T cells ($p = 0.0160$; Figures S5D–S5F). Thus, $CD4^+$ T cells secreting IFNγ and IL-17A are not present in the spleens or lymph nodes in CFA/α-syn$_{32-46}$-immunized HLA mice at 28 DPI, a response consistent with either release from these organs or loss due to cell death after *in vitro* re-stimulation.

To determine whether α-syn$_{32-46}$ immunizations induced a humoral immune response in HLA mice, we assessed the levels of antibodies that recognize α-syn$_{32-46}$ from blood at 28 DPI. In both WT and HLA mouse strains, CFA/α-syn$_{32-46}$ immunization produced high levels of antigen-specific antibodies (Figure S6I). Thus, CFA/α-syn$_{32-46}$ immunizations in DRB1*15:01 HLA mice trigger an immune response consistent with bulk RNA-seq data; however, the α-syn$_{32-46}$-specific T cells have likely left the peripheral lymphoid organs and were redistributed to other organs, potentially the ENS.

$CD4^+$ T_H1/T_H17 cells adopt a T_{RM} gene signature in the ileum of CFA/α-syn$_{32-46}$-immunized HLA mice typically found in inflamed mucosal barriers

To determine which immune cell types are responsible for the upregulated pathways identified by bulk RNA-seq of the ileum in CFA/α-syn$_{32-46}$-immunized HLA mice, we performed scRNA-seq and analysis on fluorescence-activated cell sorted (FACS) intestinal $CD45^+$ immune cells after dissociation of the small intestine from sick CFA/α-syn$_{32-46}$-, CFA-, or PBS-immunized HLA mice at 21 DPI (Figure 5A; Table S2A). We performed normalization, feature selection, and non-linear dimensional reduction of the raw gene expression data after removal of ribosomal (*Rps/l−*) and mitochondrial (*Mt−*) genes associated with technical artifacts. After quality control and filtering, 5,430 cells from PBS-injected, 9,826 cells from CFA-immunized, and 12,642 cells from CFA/α-syn$_{32-46}$-immunized HLA mice were used for downstream analysis (Table S2A). We used Harmony batch correction to integrate scRNA-seq data from three batches[43] and identified 27 unique cell clusters from the three conditions using the non-linear dimensional reduction technique uniform manifold approximation and projection (UMAP) (Figures 5D, S6A, and S6B). The UMAP analysis revealed large populations of lamina propria T cell subtypes, intraepithelial lymphocytes (IELs), and plasma cells and smaller populations of myeloid cells, innate lymphoid cells, and memory B cells isolated from the gut in each condition (Figures 5D and 5E; Table S2B).

Because CFA/α-syn$_{32-46}$ immunization in HLA mice triggered constipation and enteric neuronal loss, we postulated that α-syn-specific $CD4^+$ T cells may home to the gut, as they were not present in lymphoid tissue (Figure S5). To examine transcriptome changes in $CD4^+$ T cell subtypes after α-syn$_{32-46}$ immunization, we separated $CD4^+$ T_H1 and T_H17 cell clusters from the $CD45^+$ single cell dataset and performed differential gene expression analysis among three conditions (Figures 5F, 5H, and 5K). T_H1, and to a lesser extent T_H17, cells isolated from CFA/α-syn$_{32-46}$-immunized HLA mice upregulated a gene signature reminiscent of $CD4^+$ T_{RM} cells (high levels for *Crem*, *Vps37b*, *Ramp3*, *Ifngr1*, and *Tnfrsf4*; Figures 5G, 5I, 5J, 5L, and 5M), identified recently in the murine colon and the murine lung following viral infection.[44–47] T_H1 cells from CFA/α-syn$_{32-46}$ immunization

Figure 4. Neuronal loss begins after 18 days post immunization in CFA/α-syn$_{32-46}$-immunized HLA-DRB1*15:01 mice

(A and B) Diagram of the experimental design (A) and the MP and SP of the ileum (B) used for analysis.

(C–F) Representative images of the MP and SP at 18 DPI stained for DAPI (blue), TH (green), and ANNA1 (red).

(G and H) Dotted bar graphs depicting the number of $ANNA1^+$ (G) and TH^+ (H) neurons in the MP of CFA-only- (black circles) and CFA/α-syn$_{32-46}$-immunized (green circles) mice at 18 DPI.

(I and J) Dotted bar graphs of $ANNA1^+$ (I) and TH^+ cells (J) in the SP of CFA-only- (black) and CFA/α-syn$_{32-46}$-immunized (green) mice at 18 DPI.

(K and L) Dotted bar graphs of the TH area (K) and MFI (L) of TH signal in the SP of CFA-only- (black) and CFA/α-syn$_{32-46}$-immunized (green) mice at 18 DPI.

(M–P) Representative images of the MP and SP at 42 DPI stained for DAPI (blue), TH (green), and ANNA1 (red).

(Q and R) Dotted bar graphs of $ANNA1^+$ (Q) and TH^+ cells (R) in the MP of CFA-only- (black) and CFA/α-syn$_{32-46}$-immunized (green) mice at 42 DPI.

(S–V) Dotted bar graphs of $ANNA1^+$ (S), and TH^+ cells (T), TH area (U), and MFI (V) of TH signal in the SP of CFA-only- (black) and CFA/α-syn$_{32-46}$-immunized (green) mice at 42 DPI. Dotted bar graphs show the mean and error bars the SEM. Each symbol represents data collected from a mouse. Data were analyzed by a two-tailed Student's t test. *$p < 0.05$, **$p < 0.01$. 18 DPI: CFA only, n = 5 mice; CFA/α-syn$_{32-46}$, n = 5 mice; 42 DPI: CFA only, n = 6–7 mice, CFA/α-syn$_{32-46}$, n = 6 mice (data were collected from one experiment). (C–F and M–P) Scale bars, 50 μm. See also Figures S3 and S4.

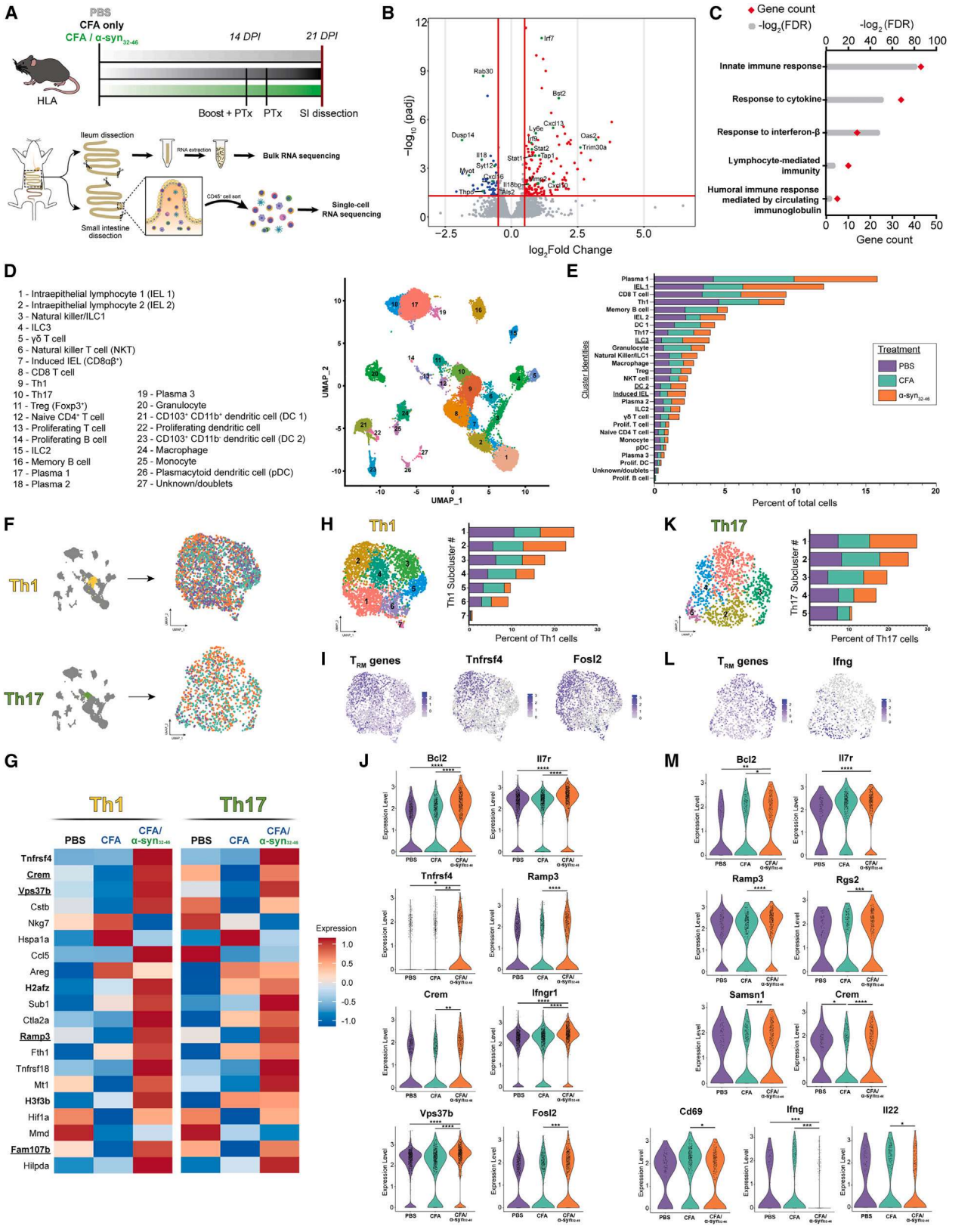

(legend on next page)

also upregulated *Fosl2* expression (Figure 5J), a gene essential for T_{RM} identity (reviewed in Yenyuwadee et al.[48]). Both T_H1/T_H17 populations upregulated pro-survival memory genes (e.g., *Bcl2* and *Il7r*; Figures 5J and 5M); however, *Id3*, a marker of $CD4^+$ memory T_H1 cells,[49] was absent from the T_H1 population in CFA/α-syn_{32-46}-immunized HLA mice, suggesting that they were not typical memory cells. We re-clustered T_H1 and T_H17 cells to identify putative subpopulations with distinct T_{RM} signatures (Figures 5H and 5K). There was an enrichment for T_{RM} gene signatures in subcluster 2 of the T_H1 population, which was over-represented by cells from the CFA/α-syn_{32-46}-immunized HLA mice (Figures 5H and 5I; Table S2B). In contrast, the T_{RM} gene signature was more dispersed among the five T_H17 subclusters (Figures 5K and 5L). The T_H1/T_H17 cell effector genes and cytokines (*Cd69*, *Ifng*, and *Il22*) were also significantly downregulated in T_H17 cells from CFA/α-syn_{32-46}-immunized mice (Figure 5M), whereas additional T_{RM} genes, such as *Rgs2*[50,51] and *Samsn1*,[45,52] were upregulated in T_H17 cells from CFA/α-syn_{32-46}-immunized HLA mice (Figure 5M). Gene-set enrichment analysis (GSEA) of T_H1 and T_H17 cells did not reveal significant GO terms enriched after CFA/α-syn_{32-46}-immunization in HLA mice. Overall, these results demonstrate that CFA/α-syn_{32-46} immunizations in HLA mice triggered transcriptome shifts in $CD4^+$ T_H1/T_H17 cells consistent with a T_{RM} phenotype, similar to the signature found in antigen-experienced T_{RM} cells at mucosal barriers following infection or chronic inflammation. These findings may explain why T_H1/T_H17 cells were not found in peripheral lymphoid organs in CFA/α-syn_{32-46}-immunized HLA mice (Figure S5).

Two populations of IELs (IEL 1, induced IEL) were predominately derived from the CFA/α-syn_{32-46}-immunized HLA mice (>45% of the cluster), even after correcting for cell numbers from other conditions (Figures 5E, S6C, S6D, and S6F; Table S2B); these populations expressed effector T cell markers and cytokines (*Itgae*, *Cd69, Gzma, Gzmb,* and *Id2*) but very few memory genes (*Id3*, *Tcf7*, *Xcl1*) (Figure S6F). The third population of IELs (IEL 2) expressed high levels of $CD8^+$ T cell memory identity (*Id3*, *Tcf7*, *Xcl1*), but lacked expression of effector cytokines (*Ifng*, *Gzma*, and *Gzmb*) (Figure S6F). In contrast to the $CD8\alpha^+$ IEL 1 cluster, the $CD8\alpha\beta^+$ induced IEL cluster is likely derived from antigen-experienced $CD8^+$ T cells which home to the intestinal epithelium following activation (reviewed in Cheroutre et al.[53]). Differential gene expression analysis of induced IELs among three conditions revealed upregulation of T_{RM}-associated genes (e.g., *Nr4a1*, *Rgs2*, and *Vps37b*) in CFA/α-syn_{32-46}-immunized HLA mice (Figures S6E and S6F). Based on this unique gene signature, the induced IELs are likely an effector-like antigen-experienced $CD8\alpha\beta^+$ IEL population[54] highly enriched in CFA/α-syn_{32-46}-immunized HLA mice. Granulocytes, composed of $CCR3^+$ eosinophils and $CXCR2^+$ neutrophils, were predominantly derived from CFA-immunized HLA mice (Figures S6G and S6H). Differential gene expression analysis revealed upregulated genes associated with granules (lipocalin-2 [*Lcn2*], *Chil3*) and the type 1 IFN response (*Ifitm1*, *Ifitm2*, *Ifitm3*, *Ifitm6*, *Irf1*, *Ifnar2*) in CFA/α-syn_{32-46}- compared with CFA-immunized HLA mice (Figures S6J and S6K). GSEA confirmed enrichment of genes for: (1) defense response to bacteria (GO: 0042742), (2) response to IFNβ (GO: 0035456), and (3) humoral immune response (GO: 0006959) (Figure S6I). Overall, the scRNA-seq analysis of immune cells shows that the immune response in the gut at peak constipation (21 DPI; Figures 5A–5C) was driven not only by $CD4^+$ T cells but also by $CD8\alpha\beta^+$ effector IEL cells and granulocytes, which likely contribute to disease outcomes.

Figure 5. Gene signatures associated with the innate and adaptive immune responses and altered T_H1/T_H17 gene signatures are present in the small intestine of α-syn_{32-46}-immunized HLA mice

(A) Diagram of the experimental design for bulk and scRNA-seq (bulk RNA sequencing: CFA only, n = 4 mice; CFA/α-syn_{32-46}, n = 4 mice. scRNA-seq: PBS, n = 2 mice; CFA, n = 3 mice; CFA/α-syn_{32-46}, n = 3 mice).

(B) A volcano plot of differentially expressed gene (DEG) from bulk RNA-seq of the ileums of CFA/α-syn_{32-46}- vs. CFA-only-immunized HLA mice at 21 DPI. Significantly downregulated (blue) and upregulated (red) genes are plotted by fold change on the x axis and the adjusted p value on the y axis. Red lines indicate adjusted p values (p_{adj}) ≤ 0.05 and $|\log_2 FC| \geq 0$. Genes of interest are highlighted in green and labeled.

(C) GO enrichment bar graph depicting five functional categories of upregulated genes from the ileum of α-syn_{32-46}-immunized HLA mice at 21 DPI. Red diamonds indicate the number of genes represented by the GO term, and gray bars indicate $-\log_2$(FDR) values.

(D) UMAP representation of scRNA-seq data of $CD45^+$ cells sorted from the small intestine of all three conditions (PBS, CFA, and CFA/α-syn_{32-46}).

(E) Bar graph of the proportion of sequenced $CD45^+$ cells for each cluster of the UMAP. Each bar shows the relative proportions of $CD45^+$ cells for each condition (PBS [purple], CFA only [teal], CFA/α-syn_{32-46} [orange]), corrected for the number of cells sequenced from each condition. The underlined clusters are over-represented (>45% of cluster) by cells isolated from CFA/α-syn_{32-46}-immunized HLA mice.

(F) UMAP projections of T_H1 and T_H17 clusters isolated from the dataset: PBS (purple), CFA only (teal), CFA/α-syn_{32-46} (orange).

(G) Heatmap of the average expression of 20 T_{RM}-associated genes in T_H1 and T_H17 cells, separated by condition. Bolded and underlined gene names are significantly upregulated in the T_H1 and T_H17 population ($p_{adj} < 0.05$) from CFA/α-syn_{32-46}-immunized HLA mice compared with CFA-only-immunized HLA mice.

(H) UMAP projection of the T_H1 cell subset with a bar graph of the proportion of T_H1 subclusters as a percent of total T_H1 cells by condition. Each bar shows the relative proportions of cells from each condition (PBS [purple], CFA only [teal], CFA/α-syn_{32-46} [orange]), corrected for the number of total T_H1 cells from each treatment.

(I) Feature plots of T_{RM} genes from (G), *Tnfrsf4*, and *Fosl2* in the T_H1 cluster.

(J) Violin plots of *Bcl2*, *Il7r*, *Tnfrsf4*, *Ramp3*, *Crem*, *Ifngr1*, *Vps37b*, and *Fosl2* gene expression in the T_H1 cluster, separated by condition. Statistical analyses were done by Wilcoxon rank sum test, followed by Bonferroni correction for multiple comparisons.

(K) UMAP projection of the T_H17 cell subset with a bar graph of the proportion of T_H17 subcluster as a percent of total T_H17 cells by condition. Each bar shows the relative proportions of cells from condition (PBS [purple], CFA only [teal], CFA/α-syn_{32-46} [orange]), corrected for the number of cells from each treatment within the T_H17 cluster.

(L) Feature plots of T_{RM} genes (G) and *Ifng* in the T_H17 cluster.

(M) Violin plots of *Bcl2*, *Il7r*, *Ramp3*, *Rgs2*, *Samsn1*, *Crem*, *Cd69*, *Ifng*, and *Il22* gene expression in the T_H17 cluster, separated by immunization treatment. For statistical significance: $^*p_{adj} < 0.05$, $^{**}p_{adj} < 0.01$, $^{***}p_{adj} < 0.001$, $^{****}p_{adj} < 0.0001$. See also Figure S6.

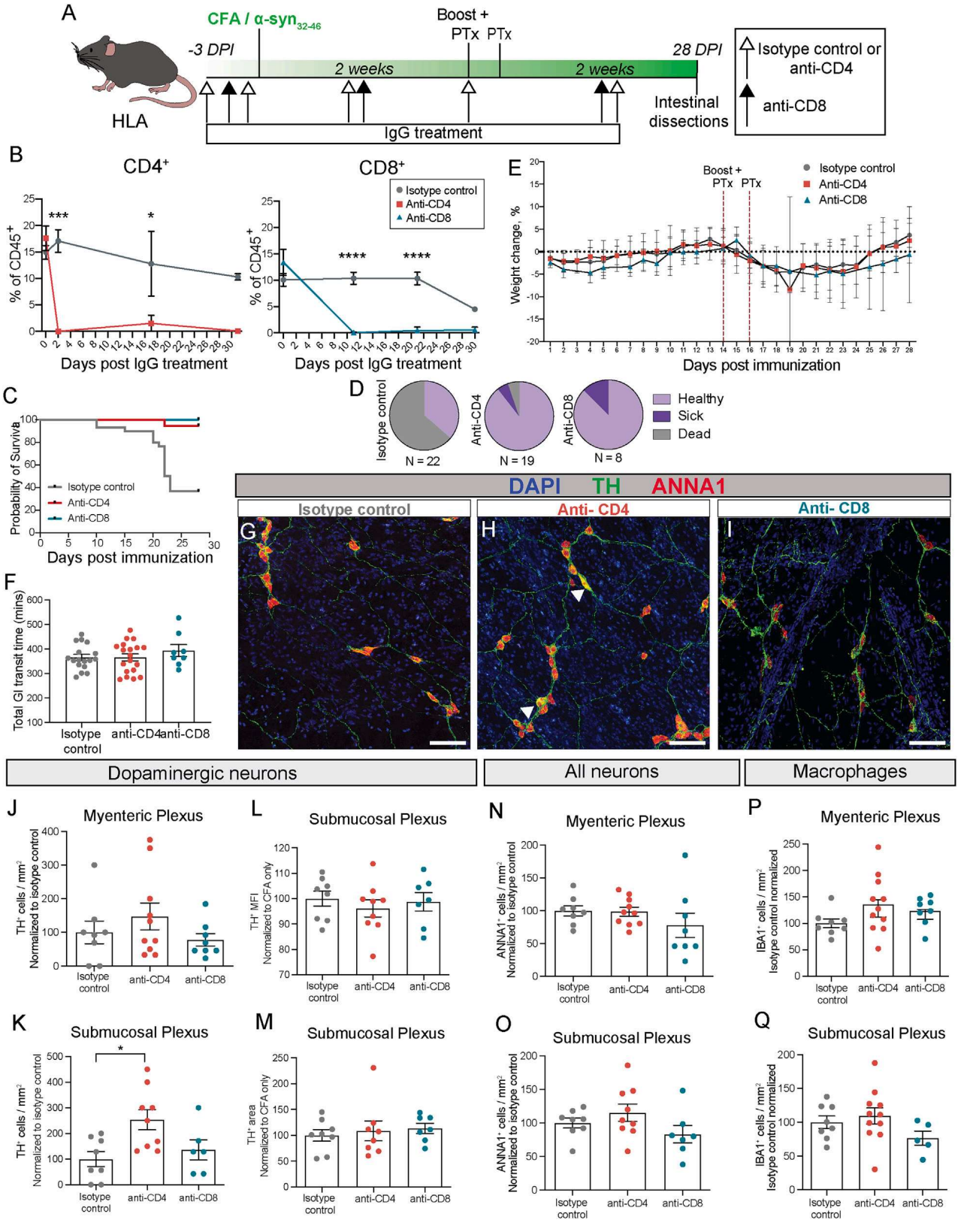

(legend on next page)

CD4$^+$ T cells are partially responsible for the ENS dopaminergic neuron damage

Because CD4$^+$ T cells and CD8αβ$^+$ effector IEL cells drive immune responses in the gut of CFA/α-syn$_{32-46}$-immunized HLA mice, we depleted either CD4$^+$ or CD8$^+$ T cells with anti-CD4, anti-CD8, or isotype control antibodies administered before and at weekly intervals after α-syn$_{32-46}$ immunization to determine their contribution to inflammation, neurodegeneration, and constipation (Figure 6A). Flow cytometry analysis of peripheral blood showed that the appropriate antibody treatments depleted CD4$^+$ and CD8$^+$ T cell types in mice (Figure 6B).

A high proportion (~64%) of CFA/α-syn$_{32-46}$-immunized HLA mice treated with the IgG isotype control did not survive to 28 DPI, while nearly all CD4$^+$- or CD8$^+$-depleted CFA/α-syn$_{32-46}$-immunized HLA mice survived until sacrifice (Figures 6C and 6D). There was no significant difference in weight loss (Figure 6E), GI transit times (Figure 6F), and macrophage number in either MPs or SPs (Figures 6P and 6Q) of all treatment groups. Importantly, histopathological analysis revealed a rescue of TH$^+$ neurons in the SP of CD4$^+$-depleted CFA/α-syn$_{32-46}$-immunized HLA mice, but no rescue with depletion of CD8$^+$ T cells (Figures 6G–6K). Interestingly, the neuronal loss appeared to be specific to TH$^+$ cells, as other ENS neurons remained unchanged across all treatment groups. Thus, CD4$^+$ T cells may be in part responsible for inducing TH$^+$ cell damage and loss after CFA/α-syn$_{32-46}$ immunizations in HLA mice, but additional cells (CD8αβ$^+$ effector IEL cells, granulocytes etc.) may contribute to other disease phenotypes (constipation and weight loss).

DISCUSSION

PD is a multifactorial disease, and dysregulation of the immune response targeting α-syn has been strongly implicated as a potential driver of pathogenesis, at least in a subset of PD patients during the first decade after diagnosis.[18–20] Our previous studies have shown that CD4$^+$ T cells that respond prominently to two regions of the α-syn protein are found in the blood of PD patients.[18] Although the immune response to the α-syn$_{32-46}$ region is restricted to patients carrying a specific HLA haplotype (B*07:02 C*07:02 DRB5*01 DRB1*15:01 DQA1*01:02 DQB1*06:02),[18] how these interactions trigger PD pathogenesis is unknown.

Using an active immunization approach in mice similar to EAE induction,[35,36] we find that α-syn$_{32-46}$ immunizations in mice in which their native MHCII allele was substituted by the human HLA-DRB1*15:01 allele recapitulate multiple aspects of the immune response seen in PD patients. These include loss of ENS neurons, a progressive decrease in dopaminergic neuronal processes in the ENS, transient weight loss, and constipation, reminiscent of gastroenterological deficits reported in PD patients 20 years prior to disease onset[5] (Figure 7). Some of these disease phenotypes (e.g., progressive decrease in dopaminergic neurons) require, in part, CD4$^+$ T cells (Figure 6), although the mechanisms by which CD4$^+$ T cells mediate them are unclear. Our findings confirm previous hypotheses that α-syn$_{32-46}$ antigen/HLA-DRB1*15:01 interactions underlie some of the features resembling prodromal PD manifested by prominent gut inflammation and CD4$^+$ T cell-driven loss of enteric neurons.

Although the immunizations generated a strong antibody response to α-syn$_{32-46}$ in both WT and HLA mice, we found that T_H1, T_H17, and CD8$^+$ T cells that responded to α-syn$_{32-46}$ were retained in spleen and axillary lymph nodes only in WT mice. Strikingly, α-syn$_{32-46}$-specific CD4$^+$ T cells were absent in immune organs in CFA/α-syn$_{32-46}$-immunized HLA mice (Figure S5). This observation is consistent with effective homing of these CD4$^+$ T cells from dedicated immune organs to the gut,[55] where they are likely responsible for inflammation, loss of ENS neurons, and constipation (Figure 7). scRNA-seq of intestinal immune cells confirmed the presence of CD4$^+$ T_H1 and T_H17 lymphocytes in the gut of CFA/α-syn$_{32-46}$-immunized mice, where these cells adopted a transcriptome signature characteristic of antigen-experienced T_{RM} cells found in mucosal barriers during infection and chronic inflammation, including IBD (reviewed in Lange et al.[56] and Lyu et al.[57]) (Figures 5G–5M).

In our humanized mouse model, constipation, a GI symptom present in the majority of PD patients, required the combination of α-syn$_{32-46}$ and the HLA DRB1*15:01 allele. Although other PD mouse models have reported constipation,[13,58] our study demonstrates that a specific combination of an α-syn-derived epitope and an HLA allele can drive gut pathology and dysmotility. This pathology is characterized by activation of innate and adaptive immune gene signatures (Figures 5B and 5C), followed initially by a loss of ANNA1$^+$ enteric neurons in the SP (28 DPI) and subsequently by a progressive reduction in TH$^+$ neuronal

Figure 6. CD4$^+$ T cell depletion partially rescues neuronal loss in α-syn$_{32-46}$-immunized HLA mice

(A) Diagram of the experimental design. Mice received α-CD4 or isotype control antibodies (white arrows) or α-CD8 antibodies (black arrows) intraperitoneally.

(B) Graph showing the levels of CD4$^+$ or CD8$^+$ T cells as % of CD45$^+$ cells at three distinct DPIs in CFA/α-syn$_{32-46}$-immunized HLA mice for each treatment: α-CD4 (red), α-CD8 (teal), or isotype control (gray).

(C) Kaplan-Meier curve depicting the probability of survival and (D) pie charts displaying the proportion of α-CD4- (red), α-CD8- (teal), and isotype-control-treated (gray) CFA/α-syn$_{32-46}$-immunized HLA mice that remained healthy (light purple), became ill (dark purple), and died (gray).

(E) Graph depicting the percent of weight change from the initial weight (0 DPI) of α-CD4- (red), α-CD8- (teal), or isotype-control-treated (gray) CFA/α-syn$_{32-46}$-immunized HLA mice.

(F) Dotted bar graph depicting the total GI transit time of α-CD4- (red), α-CD8- (teal), or isotype-control-treated (gray) CFA/α-syn$_{32-46}$-immunized HLA mice.

(G–I) Representative fluorescent images of the SP of isotype-control- (G), α-CD4- (H), and α-CD8-treated (I)CFA/α-syn$_{32-46}$-immunized HLA mice stained with DAPI (blue), TH (green), and ANNA1 (red). White arrowheads indicate TH$^+$ cell bodies. Scale bars, 100 μm.

(J–Q) Dotted bar graphs depicting the number of dopaminergic neurons (J and K), TH$^+$ MFI (L), TH$^+$ area (M), all neurons (N and O), and macrophages (P and Q) in the MP and SP of α-CD4- (red), α-CD8- (teal), or isotype-control-treated (gray) CFA/α-syn$_{32-46}$-immunized HLA mice. Data analyzed by repeated-measure ANOVA (B and C) and two-way ANOVA (G–N). Bar graphs depict the mean and error bars the SEM. Each symbol in the bar graphs represents the data collected from one mouse. *$p < 0.05$, ***$p < 0.001$, ****$p < 0.0001$. Isotype control, n = 8 mice; α-CD4, n = 10 mice; α-CD8, n = 8; data collected from 3 independent experiments. See also Figure S5.

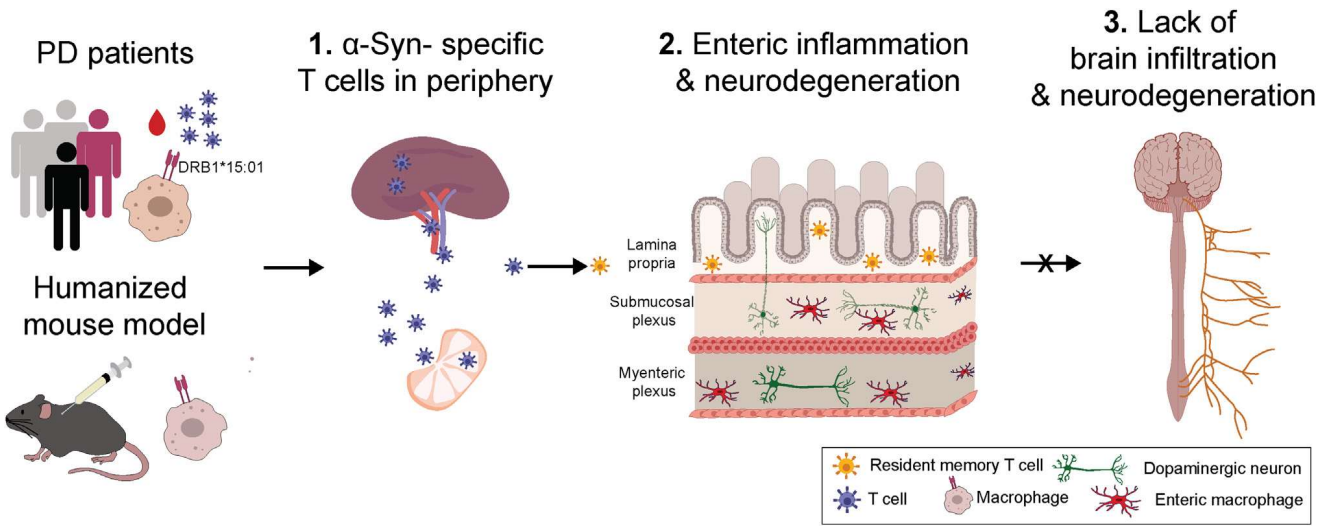

Figure 7. The role of α-syn-specific T cells in PD pathogenesis. α-Syn-specific T cells have been identified in PD patient carriers of the HLA-DRB1*15:01 allele

Humanized mice, lacking MHCII$^{-/-}$ and expressing HLA-DRB1*15:01 that are immunized with the α-syn$_{32-46}$ may produce α-syn-specific T cells (T_H1 and T_H17 lymphocytes, blue) in the peripheral lymphoid organs (spleen and lymph nodes). These T cell populations (blue) leave the circulation to home to the gut where they are converted to mucosal T_{RM} (yellow) found normally during infection or chronic inflammation based on our scRNA-seq data. In addition, signatures of innate and adaptive immune responses are upregulated in the gut with CFA/α-syn$_{32-46}$ immunizations based on bulk RNA sequencing. The activation of both innate and adaptive immune responses in CFA/α-syn$_{32-46}$-immunized HLA mice may trigger enteric neurodegeneration in the SP. There is neither inflammation nor T cell infiltration into the brains of α-syn$_{32-46}$-immunized HLA mice, suggesting that additional factors are required to induce CNS phenotypic characteristics of PD.

processes and intensity (28–42 DPI) in CFA/α-syn$_{32-46}$-immunized HLA mice (Figures 3, 4, and 7).

Depletion experiments targeting CD4$^+$ and CD8$^+$ T cells suggest that CD4$^+$ T cells are critical drivers of dopaminergic neuron damage and loss in the gut and are consistent with other studies implicating CD4$^+$ T cells in neuronal damage in other PD mouse models.[59,60] The timing of the enteric features in this model are consistent with a robust IFN response gene signature, revealed by bulk RNA-seq (Figures 5B and 5C). Although CD4$^+$ T cells promote enteric neuron loss, the relationship between CD4$^+$ T cell-mediated neuronal loss and IFN response requires further investigation. The IFN response at 21 DPI may reflect a response to dying enteric neurons from the extracellular release of nucleic acids. Type 1 IFN responses have been suggested to play a non-classical role in neurodegeneration, including in the 1-methyl-4-phenyl-1,2,3,6-tetrahydropyridine (MPTP) mouse model for PD.[61]

Our scRNA-seq has identified a population of CD4$^+$ T_{RM} cells present in the gut of sick CFA/α-syn$_{32-46}$-immunized HLA mice at 21 DPI. In human IBD, CD4$^+$ CD69$^+$ CD103$^+$ T_{RM} cells are proposed to accumulate in the gut and trigger intestinal inflammation.[57,62] A similar CD4$^+$ T_{RM} population (CD161$^+$ CCR5$^+$) produces proinflammatory cytokines in Crohn's disease.[63] Populations of CD103$^-$ CD4$^+$ T_{RM} cells similar to those identified in our scRNA-seq results have been shown to expand following antigen exposure. For example, *Aspergilus fumigatus* generates CD103$^-$ CD4$^+$ T_{RM} cells in murine lung, which produce proinflammatory cytokines and contribute to fibrosis (reviewed in Hirahara et al.[64]). In addition to CD4$^+$ T_{RM} cells, CD8$^+$ CD103$^-$ T_{RM} cells in the intestine give rise to CD8$^+$ CD103$^+$ T_{RM} cells that respond to secondary infections.[65,66] The identification of CD4$^+$ T_{RM} cells in the gut of CFA/α-syn$_{32-46}$-immunized HLA mice at 21 DPI, coupled with their critical role in IBD or Crohn's disease, suggest that they may drive ENS pathology in the ileum.

The overrepresentation of induced IELs and granulocytes from CFA/α-syn$_{32-46}$-immunized HLA mice suggests that antigen exposure may expand other immune cells in addition to CD4$^+$ T cells that are critical for the gut pathology and motility (e.g., constipation), although this is difficult to ascertain with our small sample size. Future studies with enrichment of specific immune subtypes could provide additional insights into their role in disease pathogenesis. Granulocytes isolated from CFA/α-syn$_{32-46}$-immunized mice displayed an anti-bacterial phenotype compared with the CFA-immunized mice, as the inducer of anti-bacterial inflammation *Lcn2* was highly upregulated in this population. *Lcn2* is highly expressed in intestinal inflammation, including IBD (reviewed in Moschen et al.[67]). Such robust antimicrobial responses in our immunization model may suggest the presence of a leaky gut, which could also contribute to the constipation phenotype. The IFN responses that were highly upregulated from bulk RNA-seq are largely absent from the single-cell dataset, with the exception of granulocytes from CFA/α-syn$_{32-46}$-immunized mice (Figures S6I and S6K; Table S2). Other cells in the intestine, such as epithelial cells, may produce most of the transcriptional responses detected by bulk RNA-seq of the ileum. These collective bulk and scRNA-seq data support the model that HLA-α-syn$_{32-46}$ interactions drive innate and adaptive immune responses in the gut that underlie the pathology, and α-syn-specific CD4$^+$ T cells are critical, at least in part, to drive the enteric features of prodromal PD.

The mechanisms by which CD4$^+$ T cells mediate enteric neuronal loss remain unclear, although their roles have been confirmed in rodent models of PD with prominent CNS damage.[60,68] The immune-dependent loss of dopaminergic neurites

may be transient and could be related to a temporary loss of the TH^+ marker expression,[69–71] as has been shown in other peripheral neurons,[72,73] although it has also been reported that newborn dopamine neurons may appear in the adult small intestine in response to their death.[74]

Although constipation is linked to prodromal PD, there is little analysis of the inflammatory state or neurodegeneration associated with that condition. The density of enteric neurons in the small intestine is reported to correlate with clinical features of dysmotility.[75] Although dopamine is essential for normal GI motility in rodents,[76] some biopsy studies of the gut report no difference in dopaminergic neurons between PD patients and healthy controls,[77–79] while others report changes in dopamine in IBD.[80] These analyses are of the colon, and enteric neurons are irregularly distributed across the two plexuses of the 25-foot-long human adult bowel,[81] making it challenging to analyze such specimens. Our study examines up to 1 mm^2 of MP and SP of the ileum per mouse at confocal resolution, offering a broad analysis of this enteric region. Future human studies should focus on a thorough analysis of the ENS to assess the extent of neurodegeneration throughout disease progression. Importantly, our mouse model examines gut responses to two acute immunizations with a self-antigen, in contrast to chronic antigen exposure present in PD. It is possible that ENS symptoms in PD, including constipation, might wax and wane depending on the presence of specific epitopes, particularly α-syn_{32-46} or phosphorylated S129, similar to relapsing-remitting MS.

Transient CNS entry of peripheral T cells that recognize a mitochondria-derived antigen associated with intestinal inflammation was reported to drive SN dopamine axonal loss in *Pink1*-deficient mice.[82] In contrast, we observed no CNS symptoms ($CD3^+$ T cell infiltrates, neuroinflammation, or loss of dopaminergic neurons) in the α-syn_{32-46}/HLA-DRB1*15:01 mouse model, consistent with reports that ENS symptoms appear decades prior to CNS symptoms in PD patients. The lack of CNS damage in the α-syn_{32-46}/HLA-DRB1*15:01 model suggests that a "second hit" is required to target α-syn-specific T cells into the CNS, followed by neuroinflammation and loss of central dopaminergic neurons. This could be due to the transient, rather than chronic, exposure to the α-syn epitope (two rounds of immunizations in mice in contrast to chronic exposure over decades in PD patients), or insufficient HLA-associated presentation of the α-syn_{32-46} by antigen-presenting cells in the brain, which may in turn result from disease-associated altered degradation pathways that produce neoepitopes.

In conclusion, we have shown that α-syn autoimmunity induces constipation and gut pathology, with loss of enteric neurons that can elicit symptoms that resemble those of prodromal PD. The demonstration that a restrictive HLA allele in combination with an α-syn-derived antigen leads to prodromal PD-like symptoms suggests that autoimmune responses to α-syn-derived epitopes may play an early role in PD pathogenesis.

STAR★METHODS

Detailed methods are provided in the online version of this paper and include the following:

SUPPLEMENTAL INFORMATION

Supplemental information can be found online at https://doi.org/10.1016/j.neuron.2023.07.015.

ACKNOWLEDGMENTS

We thank Michael D. Gershon, Alcmene Chalazonitis, and Wanda Setlik (CUIMC) for guidance with enteric dissections, staining, behavior experiments, and analysis of neuronal number and area in the flat mount ileum preparations; Ilir Agalliu (AECOM) for statistical analysis advice; Peter Sims (CUIMC) for guidance with scRNA-seq analysis; and Ori Lieberman, Michael Post, Charlotte Wayne, Madeline Edwards, Megan Sykes, Ai Yamamoto, and Wassim Elyaman (CUIMC) for suggestions with various experiments throughout this study. This research was funded in part by Aligning Science Across Parkinson's (#0375) through the Michael J. Fox Foundation for Parkinson's Research (MJFF). For the purpose of open access, the authors have applied a CC BY public copyright license to all Author Accepted Manuscripts arising from this submission. D.S. and E.K. are also supported by NIH/NINDS (R01 NS095435) and the JPB Foundation. T.C., S.S., and D.A. are also supported by grants from the NIH/NIMH (R01 MH112849), NIH/NIE (R01 EY033994), and the National MS Society (RG-1901-33218). D.A. and T.C. are partially supported by unrestricted gifts from the Newport Equities LLC, the Walz family, and PANDAS Network to the Department of Neurology, CUIMC.

AUTHOR CONTRIBUTIONS

F.G., D.A., A.S., and D.S. conceived the project. F.G., C.M., N.S., S.S., S.W.K., T.C., E.K., and D.A. performed the experiments and analyses. F.G., C.M., T.C., A.S., D.A., and D.S. wrote and edited the manuscript. F.G. and C.M. prepared figures and figure legends.

DECLARATION OF INTERESTS

The authors declare no competing interests.

Received: January 6, 2022
Revised: June 7, 2023
Accepted: July 24, 2023
Published: August 18, 2023

REFERENCES

1. Fahn, S., and Sulzer, D. (2004). Neurodegeneration and neuroprotection in Parkinson disease. Neurorx *1*, 139–154. https://doi.org/10.1602/neurorx.1.1.139.
2. Heinzel, S., Berg, D., Gasser, T., Chen, H., Yao, C., and Postuma, R.B.; MDS Task Force on the Definition of Parkinson's Disease (2019). Update

of the MDS research criteria for prodromal Parkinson's disease. Mov. Disord. *34*, 1464–1470. https://doi.org/10.1002/mds.27802.

3. Fasano, A., Visanji, N.P., Liu, L.W., Lang, A.E., and Pfeiffer, R.F. (2015). Gastrointestinal dysfunction in Parkinson's disease. Lancet Neurol. *14*, 625–639. https://doi.org/10.1016/S1474-4422(15)00007-1.

4. Drossman, D.A. (2006). The functional gastrointestinal disorders and the Rome III process. Gastroenterology *130*, 1377–1390. https://doi.org/10.1053/j.gastro.2006.03.008.

5. Khoo, T.K., Yarnall, A.J., Duncan, G.W., Coleman, S., O'Brien, J.T., Brooks, D.J., Barker, R.A., and Burn, D.J. (2013). The spectrum of nonmotor symptoms in early Parkinson disease. Neurology *80*, 276–281. https://doi.org/10.1212/WNL.0b013e31827deb74.

6. Braak, H., Del Tredici, K., Rüb, U., de Vos, R.A., Jansen Steur, E.N., and Braak, E. (2003). Staging of brain pathology related to sporadic Parkinson's disease. Neurobiol. Aging *24*, 197–211.

7. Stokholm, M.G., Danielsen, E.H., Hamilton-Dutoit, S.J., and Borghammer, P. (2016). Pathological alpha-synuclein in gastrointestinal tissues from prodromal Parkinson disease patients. Ann. Neurol. *79*, 940–949. https://doi.org/10.1002/ana.24648.

8. Svensson, E., Horváth-Puhó, E., Thomsen, R.W., Djurhuus, J.C., Pedersen, L., Borghammer, P., and Sørensen, H.T. (2015). Vagotomy and subsequent risk of Parkinson's disease. Ann. Neurol. *78*, 522–529. https://doi.org/10.1002/ana.24448.

9. Liu, B., Fang, F., Pedersen, N.L., Tillander, A., Ludvigsson, J.F., Ekbom, A., Svenningsson, P., Chen, H., and Wirdefeldt, K. (2017). Vagotomy and Parkinson disease: A Swedish register-based matched-cohort study. Neurology *88*, 1996–2002. https://doi.org/10.1212/WNL.0000000000003961.

10. Tysnes, O.B., Kenborg, L., Herlofson, K., Steding-Jessen, M., Horn, A., Olsen, J.H., and Reichmann, H. (2015). Does vagotomy reduce the risk of Parkinson's disease? Ann. Neurol. *78*, 1011–1012. https://doi.org/10.1002/ana.24531.

11. Peter, I., Dubinsky, M., Bressman, S., Park, A., Lu, C., Chen, N., and Wang, A. (2018). Anti-tumor necrosis factor therapy and incidence of Parkinson disease among patients with inflammatory bowel disease. JAMA Neurol. *75*, 939–946. https://doi.org/10.1001/jamaneurol.2018.0605.

12. Park, S., Kim, J., Chun, J., Han, K., Soh, H., Kang, E.A., Lee, H.J., Im, J.P., and Kim, J.S. (2019). Patients with inflammatory bowel disease are at an increased risk of Parkinson's disease: A South Korean nationwide population-based study. J. Clin. Med. *8*, 1191. https://doi.org/10.3390/jcm8081191.

13. Metzger, J.M., and Emborg, M.E. (2019). Autonomic dysfunction in Parkinson disease and animal models. Clin. Auton. Res. *29*, 397–414. https://doi.org/10.1007/s10286-018-00584-7.

14. Devos, D., Lebouvier, T., Lardeux, B., Biraud, M., Rouaud, T., Pouclet, H., Coron, E., Bruley des Varannes, S., Naveilhan, P., Nguyen, J.M., et al. (2013). Colonic inflammation in Parkinson's disease. Neurobiol. Dis. *50*, 42–48. https://doi.org/10.1016/j.nbd.2012.09.007.

15. Qin, X.Y., Zhang, S.P., Cao, C., Loh, Y.P., and Cheng, Y. (2016). Aberrations in peripheral inflammatory cytokine levels in Parkinson disease: A systematic review and meta-analysis. JAMA Neurol. *73*, 1316–1324. https://doi.org/10.1001/jamaneurol.2016.2742.

16. Pochard, C., Leclair-Visonneau, L., Coron, E., Neunlist, M., Rolli-Derkinderen, M., and Derkinderen, P. (2018). Cyclooxygenase 2 is upregulated in the gastrointestinal tract in Parkinson's disease. Mov. Disord. *33*, 493–494. https://doi.org/10.1002/mds.27237.

17. Cossais, F., Schaeffer, E., Heinzel, S., Zimmermann, J., Niesler, B., Röth, R., Rappold, G., Scharf, A., Zorenkov, D., Lange, C., et al. (2021). Expression profiling of rectal biopsies suggests altered enteric neuropathological traits in Parkinson's disease patients. J. Parkinsons Dis. *11*, 171–176. https://doi.org/10.3233/JPD-202258.

18. Sulzer, D., Alcalay, R.N., Garretti, F., Cote, L., Kanter, E., Agin-Liebes, J., Liong, C., McMurtrey, C., Hildebrand, W.H., Mao, X., et al. (2017). T cells from patients with Parkinson's disease recognize alpha-synuclein peptides. Nature *546*, 656–661. https://doi.org/10.1038/nature22815.

19. Lindestam Arlehamn, C.S., Dhanwani, R., Pham, J., Kuan, R., Frazier, A., Rezende Dutra, J., Phillips, E., Mallal, S., Roederer, M., Marder, K.S., et al. (2020). Alpha-synuclein-specific T cell reactivity is associated with preclinical and early Parkinson's disease. Nat. Commun. *11*, 1875. https://doi.org/10.1038/s41467-020-15626-w.

20. Garretti, F., Agalliu, D., Lindestam Arlehamn, C.S., Sette, A., and Sulzer, D. (2019). Autoimmunity in Parkinson's disease: the role of alpha-synuclein-specific T cells. Front. Immunol. *10*, 303. https://doi.org/10.3389/fimmu.2019.00303.

21. Fujiwara, H., Hasegawa, M., Dohmae, N., Kawashima, A., Masliah, E., Goldberg, M.S., Shen, J., Takio, K., and Iwatsubo, T. (2002). Alpha-synuclein is phosphorylated in synucleinopathy lesions. Nat. Cell Biol. *4*, 160–164. https://doi.org/10.1038/ncb748.

22. Dendrou, C.A., Petersen, J., Rossjohn, J., and Fugger, L. (2018). HLA variation and disease. Nat. Rev. Immunol. *18*, 325–339. https://doi.org/10.1038/nri.2017.143.

23. Polymeropoulos, M.H., Lavedan, C., Leroy, E., Ide, S.E., Dehejia, A., Dutra, A., Pike, B., Root, H., Rubenstein, J., Boyer, R., et al. (1997). Mutation in the alpha-synuclein gene identified in families with Parkinson's disease. Science *276*, 2045–2047. https://doi.org/10.1126/science.276.5321.2045.

24. Krüger, R., Kuhn, W., Müller, T., Woitalla, D., Graeber, M., Kösel, S., Przuntek, H., Epplen, J.T., Schöls, L., and Riess, O. (1998). Ala30Pro mutation in the gene encoding alpha-synuclein in Parkinson's disease. Nat. Genet. *18*, 106–108. https://doi.org/10.1038/ng0298-106.

25. Zarranz, J.J., Alegre, J., Gómez-Esteban, J.C., Lezcano, E., Ros, R., Ampuero, I., Vidal, L., Hoenicka, J., Rodriguez, O., Atarés, B., et al. (2004). The new mutation, E46K, of alpha-synuclein causes Parkinson and Lewy body dementia. Ann. Neurol. *55*, 164–173. https://doi.org/10.1002/ana.10795.

26. Ki, C.S., Stavrou, E.F., Davanos, N., Lee, W.Y., Chung, E.J., Kim, J.Y., and Athanassiadou, A. (2007). The Ala53Thr mutation in the alpha-synuclein gene in a Korean family with Parkinson disease. Clin. Genet. *71*, 471–473. https://doi.org/10.1111/j.1399-0004.2007.00781.x.

27. Lesage, S., Anheim, M., Letournel, F., Bousset, L., Honoré, A., Rozas, N., Pieri, L., Madiona, K., Dürr, A., Melki, R., et al. (2013). G51D alpha-synuclein mutation causes a novel parkinsonian-pyramidal syndrome. Ann. Neurol. *73*, 459–471. https://doi.org/10.1002/ana.23894.

28. Appel-Cresswell, S., Vilarino-Guell, C., Encarnacion, M., Sherman, H., Yu, I., Shah, B., Weir, D., Thompson, C., Szu-Tu, C., Trinh, J., et al. (2013). Alpha-synuclein p.H50Q, a novel pathogenic mutation for Parkinson's disease. Mov. Disord. *28*, 811–813. https://doi.org/10.1002/mds.25421.

29. Yoshino, H., Hirano, M., Stoessl, A.J., Imamichi, Y., Ikeda, A., Li, Y., Funayama, M., Yamada, I., Nakamura, Y., Sossi, V., et al. (2017). Homozygous alpha-synuclein p.A53V in familial Parkinson's disease. Neurobiol. Aging *57*. 248.e7–248.e12. https://doi.org/10.1016/j.neurobiolaging.2017.05.022.

30. Pasanen, P., Myllykangas, L., Siitonen, M., Raunio, A., Kaakkola, S., Lyytinen, J., Tienari, P.J., Pöyhönen, M., and Paetau, A. (2014). Novel alpha-synuclein mutation A53E associated with atypical multiple system atrophy and Parkinson's disease-type pathology. Neurobiol. Aging *35*. 2180.e1–2180.e5. https://doi.org/10.1016/j.neurobiolaging.2014.03.024.

31. Liu, H., Koros, C., Strohäker, T., Schulte, C., Bozi, M., Varvaresos, S., Ibáñez de Opakua, A., Simitsi, A.M., Bougea, A., Voumvourakis, K., et al. (2021). A novel SNCA A30G mutation causes familial Parkinson's disease. Mov. Disord. *36*, 1624–1633. https://doi.org/10.1002/mds.28534.

32. Hamza, T.H., Zabetian, C.P., Tenesa, A., Laederach, A., Montimurro, J., Yearout, D., Kay, D.M., Doheny, K.F., Paschall, J., Pugh, E., et al. (2010). Common genetic variation in the HLA region is associated with late-onset sporadic Parkinson's disease. Nat. Genet. *42*, 781–785. https://doi.org/10.1038/ng.642.

33. Hill-Burns, E.M., Factor, S.A., Zabetian, C.P., Thomson, G., and Payami, H. (2011). Evidence for more than one Parkinson's disease-associated variant within the HLA region. PLoS One *6*, e27109. https://doi.org/10.1371/journal.pone.0027109.

34. Kannarkat, G.T., Cook, D.A., Lee, J.K., Chang, J., Chung, J., Sandy, E., Paul, K.C., Ritz, B., Bronstein, J., Factor, S.A., et al. (2015). Common genetic variant association with altered HLA expression, synergy with pyrethroid exposure, and risk for Parkinson's disease: an observational and case-control study. NPJ Parkinsons Dis. *1*, 15002. https://doi.org/10.1038/npjparkd.2015.2.

35. Lutz, S.E., Smith, J.R., Kim, D.H., Olson, C.V.L., Ellefsen, K., Bates, J.M., Gandhi, S.P., and Agalliu, D. (2017). Caveolin1 is required for Th1 cell infiltration, but not tight junction remodeling, at the blood-brain barrier in autoimmune neuroinflammation. Cell Rep. *21*, 2104–2117.

36. Lengfeld, J.E., Lutz, S.E., Smith, J.R., Diaconu, C., Scott, C., Kofman, S.B., Choi, C., Walsh, C.M., Raine, C.S., Agalliu, I., et al. (2017). Endothelial Wnt/beta-catenin signaling reduces immune cell infiltration in multiple sclerosis. Proc. Natl. Acad. Sci. USA *114*. E1168–E1177. https://doi.org/10.1073/pnas.1609905114.

37. Finn, T.P., Jones, R.E., Rich, C., Dahan, R., Link, J., David, C.S., Chou, Y.K., Offner, H., and Vandenbark, A.A. (2004). HLA-DRB1*1501 risk association in multiple sclerosis may not be related to presentation of myelin epitopes. J. Neurosci. Res. *78*, 100–114. https://doi.org/10.1002/jnr.20227.

38. Khare, M., Mangalam, A., Rodriguez, M., and David, C.S. (2005). HLA DR and DQ interaction in myelin oligodendrocyte glycoprotein-induced experimental autoimmune encephalomyelitis in HLA class II transgenic mice. J. Neuroimmunol. *169*, 1–12. https://doi.org/10.1016/j.jneuroim.2005.07.023.

39. Li, Z.S., Pham, T.D., Tamir, H., Chen, J.J., and Gershon, M.D. (2004). Enteric dopaminergic neurons: definition, developmental lineage, and effects of extrinsic denervation. J. Neurosci. *24*, 1330–1339. https://doi.org/10.1523/JNEUROSCI.3982-03.2004.

40. Yoo, B.B., and Mazmanian, S.K. (2017). The enteric network: interactions between the immune and nervous systems of the gut. Immunity *46*, 910–926. https://doi.org/10.1016/j.immuni.2017.05.011.

41. Yang, J., Sundrud, M.S., Skepner, J., and Yamagata, T. (2014). Targeting Th17 cells in autoimmune diseases. Trends Pharmacol. Sci. *35*, 493–500. https://doi.org/10.1016/j.tips.2014.07.006.

42. Sommer, A., Marxreiter, F., Krach, F., Fadler, T., Grosch, J., Maroni, M., Graef, D., Eberhardt, E., Riemenschneider, M.J., Yeo, G.W., et al. (2018). Th17 lymphocytes induce neuronal cell death in a human iPSC-based model of Parkinson's disease. Cell Stem Cell *23*, 123–131.e6. e126. https://doi.org/10.1016/j.stem.2018.06.015.

43. Korsunsky, I., Millard, N., Fan, J., Slowikowski, K., Zhang, F., Wei, K., Baglaenko, Y., Brenner, M., Loh, P.R., and Raychaudhuri, S. (2019). Fast, sensitive and accurate integration of single-cell data with Harmony. Nat. Methods *16*, 1289–1296. https://doi.org/10.1038/s41592-019-0619-0.

44. Tanemoto, S., Sujino, T., Miyamoto, K., Moody, J., Yoshimatsu, Y., Ando, Y., Koya, I., Harada, Y., Tojo, A.O., Ono, K., et al. (2022). Single-cell transcriptomics of human gut T cells identifies cytotoxic CD4(+)CD8A(+) T cells related to mouse CD4 cytotoxic T cells. Front. Immunol. *13*, 977117. https://doi.org/10.3389/fimmu.2022.977117.

45. Miragaia, R.J., Gomes, T., Chomka, A., Jardine, L., Riedel, A., Hegazy, A.N., Whibley, N., Tucci, A., Chen, X., Lindeman, I., et al. (2019). Single-cell transcriptomics of regulatory T cells reveals trajectories of tissue adaptation. Immunity *50*, 493–504.e7. https://doi.org/10.1016/j.immuni.2019.01.001.

46. Andreatta, M., Tjitropranoto, A., Sherman, Z., Kelly, M.C., Ciucci, T., and Carmona, S.J. (2022). A CD4(+) T cell reference map delineates subtype-specific adaptation during acute and chronic viral infections. eLife *11*, e76339. https://doi.org/10.7554/eLife.76339.

47. Swarnalekha, N., Schreiner, D., Litzler, L.C., Iftikhar, S., Kirchmeier, D., Künzli, M., Son, Y.M., Sun, J., Moreira, E.A., and King, C.G. (2021). C. G. T resident helper cells promote humoral responses in the lung. Sci. Immunol. *6*, eabb6808. https://doi.org/10.1126/sciimmunol.abb6808.

48. Yenyuwadee, S., Sanchez-Trincado Lopez, J.L., Shah, R., Rosato, P.C., and Boussiotis, V.A. (2022). The evolving role of tissue-resident memory T cells in infections and cancer. Sci. Adv. *8*, eabo5871. https://doi.org/10.1126/sciadv.abo5871.

49. Shaw, L.A., Deng, T.Z., Omilusik, K.D., and Takehara, K.K. (2022). Nguyen, Q. P. & Goldrath, A. W. Id3 expression identifies CD4(+) memory Th1 cells. Proc. Natl. Acad. Sci. USA *119*, e2204254119. https://doi.org/10.1073/pnas.2204254119.

50. Li, J., Olshansky, M., Carbone, F.R., and Ma, J.Z. (2016). Transcriptional analysis of T cells resident in human skin. PLoS One *11*, e0148351. https://doi.org/10.1371/journal.pone.0148351.

51. Amezcua Vesely, M.C., Pallis, P., Bielecki, P., Low, J.S., Zhao, J., Harman, C.C.D., Kroehling, L., Jackson, R., Bailis, W., Licona-Limón, P., et al. (2019). Effector T(H)17 cells give rise to long-lived T(RM) cells that are essential for an immediate response against bacterial infection. Cell *178*, 1176–1188.e15. https://doi.org/10.1016/j.cell.2019.07.032.

52. Gaublomme, J.T., Yosef, N., Lee, Y., Gertner, R.S., Yang, L.V., Wu, C., Pandolfi, P.P., Mak, T., Satija, R., Shalek, A.K., et al. (2015). Single-cell genomics unveils critical regulators of Th17 cell pathogenicity. Cell *163*, 1400–1412. https://doi.org/10.1016/j.cell.2015.11.009.

53. Cheroutre, H., Lambolez, F., and Mucida, D. (2011). The light and dark sides of intestinal intraepithelial lymphocytes. Nat. Rev. Immunol. *11*, 445–456. https://doi.org/10.1038/nri3007.

54. Wang, Y.C., Cao, Y., Pan, C., Zhou, Z., Yang, L., and Lusis, A.J. (2023). Intestinal cell type-specific communication networks underlie homeostasis and response to Western diet. J. Exp. Med. *220*, e20221437. https://doi.org/10.1084/jem.20221437.

55. McLachlan, J.B., and Jenkins, M.K. (2007). Migration and accumulation of effector CD4+ T cells in nonlymphoid tissues. Proc. Am. Thorac. Soc. *4*, 439–442. https://doi.org/10.1513/pats.200606-137MS.

56. Lange, J., Rivera-Ballesteros, O., and Buggert, M. (2022). Human mucosal tissue-resident memory T cells in health and disease. Mucosal Immunol. *15*, 389–397. https://doi.org/10.1038/s41385-021-00467-7.

57. Lyu, Y., Zhou, Y., and Shen, J. (2022). An overview of tissue-resident memory T cells in the intestine: from physiological functions to pathological mechanisms. Front. Immunol. *13*, 912393. https://doi.org/10.3389/fimmu.2022.912393.

58. Sampson, T.R., Debelius, J.W., Thron, T., Janssen, S., Shastri, G.G., Ilhan, Z.E., Challis, C., Schretter, C.E., Rocha, S., Gradinaru, V., et al. (2016). Gut microbiota regulate motor deficits and neuroinflammation in a model of Parkinson's disease. Cell *167*, 1469–1480.e12. https://doi.org/10.1016/j.cell.2016.11.018.

59. Brochard, V., Combadière, B., Prigent, A., Laouar, Y., Perrin, A., Beray-Berthat, V., Bonduelle, O., Alvarez-Fischer, D., Callebert, J., Launay, J.M., et al. (2009). Infiltration of CD4+ lymphocytes into the brain contributes to neurodegeneration in a mouse model of Parkinson disease. J. Clin. Invest. *119*, 182–192. https://doi.org/10.1172/JCI36470.

60. Williams, G.P., Schonhoff, A.M., Jurkuvenaite, A., Gallups, N.J., Standaert, D.G., and Harms, A.S. (2021). CD4 T cells mediate brain inflammation and neurodegeneration in a mouse model of Parkinson's disease. Brain *144*, 2047–2059. https://doi.org/10.1093/brain/awab103.

61. Main, B.S., Zhang, M., Brody, K.M., Ayton, S., Frugier, T., Steer, D., Finkelstein, D., Crack, P.J., and Taylor, J.M. (2016). Type-1 interferons contribute to the neuroinflammatory response and disease progression of the MPTP mouse model of Parkinson's disease. Glia *64*, 1590–1604. https://doi.org/10.1002/glia.23028.

62. Zundler, S., Becker, E., Spocinska, M., Slawik, M., Parga-Vidal, L., Stark, R., Wiendl, M., Atreya, R., Rath, T., Leppkes, M., et al. (2019). Hobit- and Blimp-1-driven CD4(+) tissue-resident memory T cells control chronic

intestinal inflammation. Nat. Immunol. *20*, 288–300. https://doi.org/10.1038/s41590-018-0298-5.

63. Yokoi, T., Murakami, M., Kihara, T., Seno, S., Arase, M., Wing, J.B., Søndergaard, J.N., Kuwahara, R., Minagawa, T., Oguro-Igashira, E., et al. (2023). Identification of a unique subset of tissue-resident memory CD4(+) T cells in Crohn's disease. Proc. Natl. Acad. Sci. USA *120*, e2204269120. https://doi.org/10.1073/pnas.2204269120.
64. Hirahara, K., Kokubo, K., Aoki, A., Kiuchi, M., and Nakayama, T. (2021). The role of CD4(+) resident memory T cells in local immunity in the mucosal tissue – protection versus pathology. Front. Immunol. *12*, 616309. https://doi.org/10.3389/fimmu.2021.616309.
65. von Hoesslin, M., Kuhlmann, M., de Almeida, G.P., Kanev, K., Wurmser, C., Gerullis, A.K., Roelli, P., Berner, J., and Zehn, D. (2022). Secondary infections rejuvenate the intestinal CD103(+) tissue-resident memory T cell pool. Sci. Immunol. *7*, eabp9553. https://doi.org/10.1126/sciimmunol.abp9553.
66. Fung, H.Y., Teryek, M., Lemenze, A.D., and Bergsbaken, T. (2022). CD103 fate mapping reveals that intestinal CD103(-) tissue-resident memory T cells are the primary responders to secondary infection. Sci. Immunol. *7*, eabl9925. https://doi.org/10.1126/sciimmunol.abl9925.
67. Moschen, A.R., Adolph, T.E., Gerner, R.R., Wieser, V., and Tilg, H. (2017). Lipocalin-2: A master mediator of intestinal and metabolic inflammation. Trends Endocrinol. Metab. *28*, 388–397. https://doi.org/10.1016/j.tem.2017.01.003.
68. Harms, A.S., Ferreira, S.A., and Romero-Ramos, M. (2021). Periphery and brain, innate and adaptive immunity in Parkinson's disease. Acta Neuropathol. *141*, 527–545. https://doi.org/10.1007/s00401-021-02268-5.
69. Soriano, M.A., Justicia, C., Ferrer, I., Rodríguez-Farré, E., and Planas, A.M. (1997). Striatal infarction in the rat causes a transient reduction of tyrosine hydroxylase immunoreactivity in the ipsilateral substantia nigra. Neurobiol. Dis. *4*, 376–385. https://doi.org/10.1006/nbdi.1997.0166.
70. Hotchkiss, A.J., and Gibb, J.W. (1980). Long-term effects of multiple doses of methamphetamine on tryptophan hydroxylase and tyrosine hydroxylase activity in rat brain. J. Pharmacol. Exp. Ther. *214*, 257–262.
71. Harvey, D.C., Lacan, G., Tanious, S.P., and Melega, W.P. (2000). Recovery from methamphetamine induced long-term nigrostriatal dopaminergic deficits without substantia nigra cell loss. Brain Res. *871*, 259–270. https://doi.org/10.1016/s0006-8993(00)02439-2.
72. Coulombe, J.N., and Bronner-Fraser, M. (1986). Cholinergic neurones acquire adrenergic neurotransmitters when transplanted into an embryo. Nature *324*, 569–572. https://doi.org/10.1038/324569a0.
73. Wolinsky, E., and Patterson, P.H. (1983). Tyrosine hydroxylase activity decreases with induction of cholinergic properties in cultured sympathetic neurons. J. Neurosci. *3*, 1495–1500.
74. Kulkarni, S., Micci, M.A., Leser, J., Shin, C., Tang, S.C., Fu, Y.Y., Liu, L., Li, Q., Saha, M., Li, C., et al. (2017). Adult enteric nervous system in health is maintained by a dynamic balance between neuronal apoptosis and neurogenesis. Proc. Natl. Acad. Sci. USA *114*. E3709–E3718. https://doi.org/10.1073/pnas.1619406114.
75. Boschetti, E., Malagelada, C., Accarino, A., Malagelada, J.R., Cogliandro, R.F., Gori, A., Bonora, E., Giancola, F., Bianco, F., Tugnoli, V., et al. (2019). Enteric neuron density correlates with clinical features of severe gut dysmotility. Am. J. Physiol. Gastrointest. Liver Physiol. *317*. G793–G801. https://doi.org/10.1152/ajpgi.00199.2019.
76. Li, Z.S., Schmauss, C., Cuenca, A., Ratcliffe, E., and Gershon, M.D. (2006). Physiological modulation of intestinal motility by enteric dopaminergic neurons and the D2 receptor: analysis of dopamine receptor expression, location, development, and function in wild-type and knock-out mice. J. Neurosci. *26*, 2798–2807. https://doi.org/10.1523/JNEUROSCI.4720-05.2006.
77. Lebouvier, T., Neunlist, M., Bruley des Varannes, S., Coron, E., Drouard, A., N'Guyen, J.M., Chaumette, T., Tasselli, M., Paillusson, S., Flamand, M., et al. (2010). Colonic biopsies to assess the neuropathology of Parkinson's disease and its relationship with symptoms. PLOS One *5*, e12728. https://doi.org/10.1371/journal.pone.0012728.
78. Annerino, D.M., Arshad, S., Taylor, G.M., Adler, C.H., Beach, T.G., and Greene, J.G. (2012). Parkinson's disease is not associated with gastrointestinal myenteric ganglion neuron loss. Acta Neuropathol. *124*, 665–680. https://doi.org/10.1007/s00401-012-1040-2.
79. Corbillé, A.G., Coron, E., Neunlist, M., Derkinderen, P., and Lebouvier, T. (2014). Appraisal of the dopaminergic and noradrenergic innervation of the submucosal plexus in PD. J. Parkinsons Dis. *4*, 571–576. https://doi.org/10.3233/JPD-140422.
80. Kurnik-Łucka, M., Pasieka, P., Łączak, P., Wojnarski, M., Jurczyk, M., and Gil, K. (2021). Gastrointestinal dopamine in inflammatory bowel diseases: A systematic review. Int. J. Mol. Sci. *22*, 12932. https://doi.org/10.3390/ijms222312932.
81. Rao, M., and Gershon, M.D. (2016). The bowel and beyond: the enteric nervous system in neurological disorders. Nat. Rev. Gastroenterol. Hepatol. *13*, 517–528. https://doi.org/10.1038/nrgastro.2016.107.
82. Matheoud, D., Cannon, T., Voisin, A., Penttinen, A.M., Ramet, L., Fahmy, A.M., Ducrot, C., Laplante, A., Bourque, M.J., Zhu, L., et al. (2019). Intestinal infection triggers Parkinson's disease-like symptoms in Pink1(-/-) mice. Nature *571*, 565–569. https://doi.org/10.1038/s41586-019-1405-y.
83. Margolis, K.G., Li, Z., Stevanovic, K., Saurman, V., Israelyan, N., Anderson, G.M., Snyder, I., Veenstra-VanderWeele, J., Blakely, R.D., and Gershon, M.D. (2016). Serotonin transporter variant drives preventable gastrointestinal abnormalities in development and function. J. Clin. Invest. *126*, 2221–2235. https://doi.org/10.1172/JCI84877.
84. Krogman, A., Tilahun, A., David, C.S., Chowdhary, V.R., Alexander, M.P., and Rajagopalan, G. (2017). HLA-DR polymorphisms influence in vivo responses to staphylococcal toxic shock syndrome toxin-1 in a transgenic mouse model. HLA *89*, 20–28. https://doi.org/10.1111/tan.12930.
85. Kimball, E.S., Palmer, J.M., D'Andrea, M.R., Hornby, P.J., and Wade, P.R. (2005). Acute colitis induction by oil of mustard results in later development of an IBS-like accelerated upper GI transit in mice. Am. J. Physiol. Gastrointest. Liver Physiol. *288*. G1266–G1273. https://doi.org/10.1152/ajpgi.00444.2004.
86. Ivanov, I.I., McKenzie, B.S., Zhou, L., Tadokoro, C.E., Lepelley, A., Lafaille, J.J., Cua, D.J., and Littman, D.R. (2006). The orphan nuclear receptor RORgammat directs the differentiation program of proinflammatory IL-17+ T helper cells. Cell *126*, 1121–1133. https://doi.org/10.1016/j.cell.2006.07.035.
87. Hao, Y., Hao, S., Andersen-Nissen, E., Mauck, W.M., 3rd, Zheng, S., Butler, A., Lee, M.J., Wilk, A.J., Darby, C., Zager, M., et al. (2021). Integrated analysis of multimodal single-cell data. Cell *184*, 3573–3587.e29. https://doi.org/10.1016/j.cell.2021.04.048.

STAR★METHODS

KEY RESOURCES TABLE

REAGENT or RESOURCE	SOURCE	IDENTIFIER
Antibodies		
Anti-tyrosine hydroxylase antibody	Millipore	Cat# AB152; RRID:AB_390204
Hamster anti mouse CD3 antibody	Bio-Rad	Cat# MCA2690; RRID:AB_905951
ANNA1	Margolis et al.[83]	V.A. Lennon, Mayo Clinic College of Medicine Cat #Hu; RRID:AB_2314657
Anti Iba1	FUJIFILM Wako Shibayagi	Cat# 019-19741; RRID:AB_839504
CD68 antibody [FA-11]	Abcam	Cat# ab53444; RRID:AB_869007
Ultra-LEAF™ Purified anti-mouse CD4 Antibody	BioLegend	Cat# 100457; RRID:AB_2810318
Ultra-LEAF™ Purified Rat IgG2b isotype control Antibody	BioLegend	Cat# 400644; RRID:AB_11149687
Ultra-LEAF™ Purified anti-mouse CD8 Antibody	BioLegend	Cat# 100746; RRID:AB_11147171
Fixable viability dye eFluor 780	eBiosciences	Cat #65-0865
Rat Anti-Mouse CD3 Molecular Complex Monoclonal Antibody, PerCP-Cy5.5 Conjugated, Clone 17A2	BD Biosciences	Cat# 560527; RRID:AB_1727463
BV421 Rat anti-mouse CD4	BD Biosciences	Cat# 562891; RRID:AB_2737870
Brilliant Violet 605(TM) anti-mouse CD8a antibody	Biolegend	Cat# 100743; RRID:AB_2561352
APC Rat anti-mouse IFN-g	BD Biosciences	Cat# 554413; RRID:AB_398551
Rat Anti-IL-17 Monoclonal Antibody, Phycoerythrin Conjugated, Clone TC11-18H10.1	BD Biosciences	Cat# 559502; RRID:AB_397256
CD45 Monoclonal Antibody (30-F11), PerCP-Cyanine5.5, eBioscience™	Thermo Fisher Scientific	Cat# 45-0451-80; RRID:AB_906233
Goat Anti-Mouse IgG H&L (HRP) antibody	Abcam	Cat# ab205719; RRID:AB_2755049
Goat anti-Rat IgG (H+L) Cross-Adsorbed Secondary Antibody, Alexa Fluor™ 647	Invitrogen	Cat# A-21247; RRID:AB_141778
Goat anti-Rabbit IgG (H+L) Cross-Adsorbed Secondary Antibody, Alexa Fluor™ 594	Invitrogen	Cat# A-11012; RRID:AB_2534079
Goat anti-Human IgG (H+L) Cross-Adsorbed Secondary Antibody, Alexa Fluor™ 594	Invitrogen	Cat# A-11014; RRID:AB_2534081
Goat anti-Armenian Hamster IgG (H+L) Highly Cross-Adsorbed Secondary Antibody, Alexa Fluor™ 488	Invitrogen	Cat# A78963; RRID:AB_2925786
Goat anti-Rabbit IgG (H+L) Highly Cross-Adsorbed Secondary Antibody, Alexa Fluor™ 647	Invitrogen	Cat# A-21245; RRID:AB_141778
Chemicals, peptides, and recombinant proteins		
EndoClear™ human recombinant a-Synuclein protein	AnaSpec	Cat #as-55555; Accession # NP_000336
α -syn$_{32-46}$ (KTKEGVLYVGSKTKE)	A&A peptides	N/A
Pertussis Toxin from *B. pertussis*, Lyophilized (Salt-Free)	List Labs	Cat #181
Complete Freund Adjuvant (CFA) containing 200 µg of *M. tuberculosis* H37Ra	BD Difco Adjuvant, Fisher Scientific	Cat #DF0638-60-7

(*Continued on next page*)

Continued		
REAGENT or RESOURCE	SOURCE	IDENTIFIER
Carmine (powder)	Millipore- Sigma	Cat #C1022
Concanavalin A	Millipore-Sigma	Cat #C2010
Critical commercial assays		
Mouse IFN-gamma DuoSet ELISA	R&D systems	Cat #DY485
Mouse IL-17A DuoSet ELISA	R&D systems	Cat #DY421
Experimental models: Organisms/strains		
Mouse: HLA DRB1*15:01 in C57BL/6J background	Krogman et al.[84]	N/A
Mouse: C57BL/6J	The Jackson Laboratory	Strain #000664; RRID:IMSR_JAX:000664
Oligonucleotides		
Primers for hygromycin control. Forward: ctgatcgaaaagttcgacagc, Reverse: gtattgaccgattccttccg	IDT	N/A
Primers for DRalpha. Forward: ccgagctctactgact, Reverse: gacttacttcagtttgtgg	IDT	N/A
Primers for DR2beta. Forward: tcgccgctgcactgtgaag, Reverse: tcctgtggcagcctaagag	IDT	N/A
Software and algorithms		
Fiji	ImageJ	Version 2.0.0, RRID:SCR_002285, https://imagej.net/software/fiji/
Prism v9.0	GraphPad	Version 9.0, RRID:SCR_002798, https://www.graphpad.com/scientific-software/prism/
DESeq2R	R package	Version 1.40.2, RRID:SCR_015687, https://bioconductor.org/packages/release/bioc/html/DESeq2.html
Deposited data		
Bulk RNA-sequencing data	this paper	NCBI GEO: GSE231873
Single-cell RNA-sequencing data	this paper	NCBI GEO: GSE233572
Mouse weight changes	this paper	Zenodo: https://doi.org/10.5281/zenodo.8144337
Gastrointestinal transit times	this paper	Zenodo: https://doi.org/10.5281/zenodo.8144320
Enteric neuron and macrophage quantifications	this paper	Zenodo: https://doi.org/10.5281/zenodo.8139875
Enteric neuron and macrophage quantifications upon T cell depletion	this paper	Zenodo: https://doi.org/10.5281/zenodo.8144253
Code for RNA-sequencing analysis in R	this paper	Zenodo: https://doi.org/10.5281/zenodo.8152796

RESOURCE AVAILABILITY

Lead contact

Further information and requests for resources and reagents should be directed to and will be fulfilled by the lead contact, David Sulzer (ds43@cumc.columbia.edu).

Materials availability

This study did not generate new unique reagents.

Data and code availability

- Microscopy reported in this paper will be shared by the lead contact upon request. RNA-sequencing data is available on the NCBI Gene Expression Omnibus (GEO) database: GSE231873 for bulk RNA-seq and NCBI GEO: GSE233572 for scRNAseq.

Datasets for mouse weight changes (Zenodo: https://doi.org/10.5281/zenodo.8144337), gastrointestinal transit time (Zenodo: https://doi.org/10.5281/zenodo.8144320), enteric neuron and macrophage quantifications (Zenodo: https://doi.org/10.5281/zenodo.8139875), and enteric neuron and macrophage quantifications upon T cell depletion (Zenodo: https://doi.org/10.5281/zenodo.8144253) are available on the Zenodo repository.

- Code for bulk and single-cell RNA-sequencing analysis is available at Zenodo: https://doi.org/10.5281/zenodo.8152796.
- Any additional information required to reanalyze data reported in this paper is available from the lead contact upon request.

EXPERIMENTAL MODEL AND SUBJECT DETAILS

Mice

All experimental procedures were approved by the Institutional Animal Care and Use Committee (IACUC) at Columbia University Irving Medical Center (CUIMC). Generation of transgenic mice expressing the *HLA DRB1*15:01* α and β chains in the C57BL/6 background have been previously described.[84] Wild-type C57BL/6J were from Jackson Laboratory (Bar Harbor, ME). The HLA transgenic mice lacking mouse MHC-II were backcrossed to the C57BL/6J strain (Jackson Laboratory) for more than 8 generations. All mice were bred within the barrier facility of CUIMC and group housed, fed regular chow. Both female and male mice were used in this study in equal numbers at the ages described in the text. No influence or association of sex was found in the results of this study.

METHOD DETAILS

Immunizations

8- to 12-week-old male and female mice were immunized subcutaneously with a 100 μl emulsion of 100 μg α-syn$_{32-46}$ peptide (A&A peptides; San Diego, CA) dissolved in PBS with Complete Freund Adjuvant (CFA) containing 200 μg *M. tuberculosis* H37Ra (BD Difco Adjuvant, Fisher Scientific, Cat #DF0638-60-7; Waltham, MA). The day of immunization was designated as day 0. Mice received a boost with the same immunization dose two weeks later. Mice received intravenous injections of 400 ng of *B. pertussis* toxin (List Biological Laboratories, Cat #181; Campbell, CA) 14- and 16-days post-initial immunization (day 0 and 2 post boost). Control animals received *B. pertussis* toxin and emulsion containing PBS/CFA without the protein or the α-syn peptide. Additional control mice received subcutaneous injections of PBS only. Mice were monitored for weight, food and fluid intake and neurological deficits and weights were recorded daily. Mice were classified as sick if they displayed 12% reduction from 0 DPI weight and/or hunched posture with ruffled and ungroomed fur (Protocols.io: dx.doi.org/10.17504/protocols.io.e6nvwd5bwlmk/v1).

Gut dissections

Mice were perfused with PBS and segments of the ileum were collected in PBS. The contents were flushed with PBS and the preparations were dissected along the mesenteric border. The flat tissue was stretched tautly and pinned flat on Sylgard (Sylgard™ 184, Dow Corning, Cat #240-4019862; Midland, MI) with the mucosa surface facing up. Specimens were fixed for one hour at room temperature 4% paraformaldehyde and washed three times with PBS for a total of 30 min. The mucosa and submucosal plexus were removed by microdissection and the mucosal was separated from the submucosal layer. The longitudinal muscles were dissected from the specimen to reveal the myenteric plexus. The submucosal and myenteric plexuses were collected and store in PBS at 4°C until immunofluorescence staining.

Intestinal flat mount immunofluorescence staining and analysis

Staining

For immunofluorescence analysis, intestinal flat mounts were blocked and permeabilized for 1 hour at room temperature with 10% normal donkey serum (Jackson Immunoresearch, Cat #017-000-121; West Grove, PA) and 1% Triton-X in PBS. Intestinal flat mounts were then incubated overnight at room temperature with primary antibodies in 10% normal donkey serum, 1% Triton-X in PBS. Sections were stained with antibodies against tyrosine hydroxylase (TH) (1:500, Millipore-Sigma, Cat # AB152; Burlington, MA) and CD3 (1:400, Bio-Rad Laboratories, Cat #MCA2690; Hercules, CA), ANNA1 (1:32,000; kind gift by the Gershon laboratory[83]), Iba1 (1:500, WAKO, Cat # 019-19741; Richmond, VA), CD68 (1:1000, Abcam, Cat # ab53444; Waltham, MA). Secondary antibodies with the appropriate conjugated fluorophores were purchased from Invitrogen. Images were acquired with an LSM700 confocal microscope and processed with Fiji software (ImageJ, NIH; Bethesda, MD) (Protocols.io: dx.doi.org/10.17504/protocols.io.q26g7p85kgwz/v1).

Acquisition

For enteric neuron imaging, both the myenteric (MP) and submucosal plexus (SP) for each mouse were analyzed. Within each plexus of each animal, 2-3, 2x2 tile z-stack 640.17x 640.17 μm confocal images at 20x magnification were acquired. This totaled to over 1 mm^2 of flat-mount enteric tissue imaged and analyzed per mouse. For imaging macrophages, both the MP and SP were analyzed for each animal. Within each plexus of each animal, 2-3, z-stack 390.09 x 390.09 μm confocal images at 20x magnification were acquired.

Analysis

The investigator who analyzed the images was blinded to each condition. The number of ANNA1$^+$, TH$^+$ cells, and IBA1$^+$ cells were counted for each image within each layer. Within the SP, the TH$^+$ signal was thresholded and the area and MFI of the thresholded TH$^+$ signal was analyzed for mean fluorescent intensity and size of area. The thresholding was consistent across each image, animal, and condition within each experiment. Within each animal, the number of ANNA1$^+$, TH$^+$ cells, and IBA1$^+$ cells across all images were summed and divided by acquisition area. Within each experiment, the cell numbers were normalized to CFA only.

Total GI transit

Carmine red, which cannot be absorbed from the gut lumen, was used to measure gastrointestinal (GI) transit time.[85] Carmine red (300 μl; 6%; Sigma-Aldrich, Cat #C1022; St Louis, MO) suspended in 0.5% methylcellulose (Sigma-Aldrich, Cat #M0512; St Louis, MO) was administered by gavage through a 21-gauge round-tip feeding needle. The time at which gavage took place was recorded as T_0. After gavage, fecal pellets were monitored at 10 min intervals for the presence of carmine red. Total GI transit time was considered as the interval between T_0 and the time of first observance of carmine red in the stool (Protocols.io: dx.doi.org/10.17504/protocols.io.4r3l22464l1y/v1).

Bulk RNA sequencing of the ileum

Ileum samples were incubated in TRIzol reagent (Thermo Fisher Scientific, Cat #15596026; Waltham, MA) and stored at -80°C. Total RNA was extracted and assessed for quality utilizing Agilent bioanalyzer for quantitation of RNA/DNA/protein (CUIMC Molecular Pathology Core). cDNA library preparation and RNA sequencing were performed by the CUIMC Genome Center. mRNAs were enriched from total RNA samples with poly-A pull-down, then processed with library construction using Illumina TruSeq chemistry. Libraries were sequenced using Illumina NovaSeq6000 at CUIMC Genome Center. Samples were multiplexed in each lane, which yielded targeted number of paired-end 100bp reads per sample. RTA (Illumina) for base calling and bcl2fastq2 (v2.19, RRID:SCR_015058, https://support.illumina.com/sequencing/sequencing_software/bcl2fastq-conversion-software.html) were used for converting BCL to fastq format, coupled with adaptor trimming. A pseudoalignment was performed to a kallisto index created from transcriptomes (GRCm38) using kallisto (v0.44.0, RRID:SCR_016582, https://pachterlab.github.io/kallisto/about). Differentially expressed genes under various conditions were tested using DESeq2 packages in R (v4.1.3, RRID:SCR_001905, http://www.r-project.org/) designed to test differential expression between two experimental groups from RNA-seq counts data. Genes were considered differentially expressed if they had an adjusted p-value <0.05 and a $\log_2$fold change below or above 0.5. The differential expression was normalized for each gene (Protocols.io: dx.doi.org/10.17504/protocols.io.rm7vzx362gx1/v1).

Single cell RNA sequencing of the ileum

Isolation of intestinal immune cells. Methods used for isolation of intestinal immune cells were adapted from Ivanov et al.[86] Briefly, mice were perfused with PBS and the small intestine removed. Peyer's patches were dissected from the small intestines, and the intestine cut open longitudinally. Intestinal contents were removed by scraping along the tissue with rounded forceps, followed by 5-6 washes with cold PBS. The intestine was cut into large fragments, placed in 5-10 ml of cell dissociation solution (5mM EDTA, 10mM HEPES, in HBSS supplemented with 2.5% FBS) and incubated for 10 minutes at 37°C rotating at 100 rpm. After 10 minutes, the solution was vortexed for 25 seconds, then the supernatant was collected and discarded using a wire mesh to collect the tissue. The tissue was incubated again in fresh cell dissociation solution, then the additional supernatant was discarded as previously described. The tissue fragments were rinsed in HBSS then cut into small pieces (~1 mm^2). The small fragments were incubated in three 20-minute intervals at 37 C with slow rotation in 5 ml of digestion solution (0.5 mg/mL collagenase D (Roche, Cat# 11088858001; Mannheim, Germany), 0.5 U/mL Dispase (Stem Cell Technologies, Cat# 07913; Vancouver, Canada), 0.5 mg/mL DNase I (Roche, Cat# 10104159001; Mannheim, Germany), in RPMI supplemented with 5% FBS). After each 20-minute digestion period, the solution was vortexed for 30 seconds, then the supernatant was collected by filtering through a 100 μm strainer. The remaining tissue fragments were placed in new digestion solution for subsequent washes. All supernatants were combined then resuspended with 10 mL of 40% Percoll (Sigma-Aldrich, Cat# GE17-0891-01; St. Louis, MO) in RPMI with 10% FBS. The resuspended cells were gently added on top of 5 mL 80% Percoll in RPMI with 10% FBS in a 15 ml conical tube. The tubes were centrifuged at 2500 rpm for 20 minutes without brake. The cell layer at the interface between 40% and 80% Percoll was collected, diluted in RPMI with 10% FBS. The cells were pelleted, then resuspended in FACS buffer, consisting of 1% bovine serum albumin (Sigma-Aldrich, Cat# A9647-100G; St. Louis, MO) in PBS (Protocols.io: dx.doi.org/10.17504/protocols.io.ewov1q42ogr2/v1).

FACS. The cells isolated from the small intestine were resuspended with 400 μl Fc block (BD Biosciences, Cat# 553142; Franklin Lakes, NJ), 1:200 in FACS buffer, and incubated for 20 minutes on ice. The cells were washed in 500 μl FACS buffer, pelleted at 1500 rpm for 2 minutes, then resuspended in 600 μl of FACS buffer with 1:100 CD45 BUV395 antibody (BD Biosciences, Cat# 564279; Franklin Lakes, NJ) and incubated on ice for 30 minutes. After 30 minutes, the cells were washed in 500 μl FACS buffer, then resuspended in 500 μl of FACS buffer containing propidium iodide (BioLegend, Cat# 421301; San Diego, CA) at 1:10,000. Viable, CD45$^+$ cells were sorted by the Sony MA900 Multi-Application Cell Sorter (Protocols.io: dx.doi.org/10.17504/protocols.io.36wgq3465lk5/v1).

Analysis. The isolated CD45$^+$ intestinal immune cells were processed by the Single Cell Analysis Core at Columbia University using the TruSeq Stranded mRNA Library Prep Kit (Illumina) and sequenced on an Illumina NovSeq 6000 platform. The Single Cell Analysis

Core used 10X Cell Ranger analysis software (v5.0.1, RRID:SCR_017344, https://support.10xgenomics.com/single-cell-gene-expression/software/pipelines/latest/installation) to process fastq files using "cellranger count" for each sample individually with default parameters producing an alignment of reads to the mm10-2020-A transcriptome. The gene-cell matrices were processed, including normalization, scaling, selection of features, linear dimensional analysis, and clustering, using the Seurat package (v4.0.0, RRID:SCR_016341, https://satijalab.org/seurat/get_started.html) in R Studio.[87] For quality control, cells with fewer than 15% mitochondrial reads and UMI counts between 1000 and 50000 were kept for downstream analysis. Ribosome (*Rps/l-*) and mitochondria (*Mt-*) associated genes were regressed from the dataset to remove effects of technical artifacts of the cell dissociation process. Batch correction was performed with the Harmony package (v0.1.1, RRID:SCR_023543, https://portals.broadinstitute.org/harmony/).[43] UMAP clusters were manually annotated by assessment of differentially expressed features using the FindMarkers function in the Seurat package (Figure S6B; Table S2C).

T cell depletions

Mice were injected interperitoneally with 250 μg of Ultra-LEAF Purified anti-mouse CD4 or Rat IgG2b isotype control antibodies (Biolegend, Cat #100457 and Cat #400644; San Diego, CA) 3 and 1 days prior to immunization. After immunization, mice were injected with 250 ug of antibody weekly. Cell depletion was assessed via flow cytometry. For depletion of $CD8^+$ T cells, mice were injected interperitoneally with 250 μg of Ultra-LEAF Purified $CD8^+$ or Rat IgG2b isotype control antibodies (Biolegend Cat # 100746 and Cat #400644; San Diego, CA) 2 days prior to immunization. After immunization, mice were injected with 250 ug of each antibody 9- and 19-days post immunization, amd cell depletion was determined via flow cytometry (Protocols.io: dx.doi.org/10.17504/protocols.io.rm7vzx372gx1/v1).

QUANTIFICATION AND STATISTICAL ANALYSIS

Fiji software (ImageJ, NIH; Bethesda, MD) was utilized for the quantitation of immunofluorescence images. Statistical analysis was performed using GraphPad Prism software version 8.0 (Graphpad Software Inc; San Diego, CA). For enteric immunofluorescence analysis, we compared $ANNA1^+$ and TH^+ cell density and TH^+ area and MFI among 3 immunization groups: PBS, CFA only, or CFA/α-syn_{32-46} using one way analysis of variance (ANOVA). In addition, we used Scheffe method for multiple comparisons given that 3 groups had unequal sample size. We fitted a general linear regression with immunization group as exposure and adjusted for variability from two different raters (FG vs. CM). All tests were 2-sided with significant level set at $p<0.05$. For all other analyses, unpaired t test was used to compare the differences between two groups in studies. One-way and two-way ANOVA followed by Bonferroni post hoc tests were performed to compare the differences among groups. Differences between groups were presented as the mean ± SEM or SD as noted in the figure legends. The sample size (n) for each experiment is indicated in figure legends and the results section. All tests were two sided and p values < 0.05 were considered to be statistically significant.